Statistical survey on the magnetic structure in magnetotail current sheets

Z. J. Rong,[1,2] W. X. Wan,[1] C. Shen,[2] X. Li,[3] M. W. Dunlop,[4] A. A. Petrukovich,[5] T. L. Zhang,[6,7] and E. Lucek[8]

Received 21 January 2011; revised 18 May 2011; accepted 21 June 2011; published 21 September 2011.

[1] On the basis of the multipoint magnetic observations of Cluster in the region 15–19 R_E downtail, the magnetic field structure in magnetotail current sheet (CS) center is statistically surveyed. It is found that the B_y component (in GSM coordinates) is distributed mainly within $|B_y| < 5nT$, while the B_z component is mostly positive and distributes mainly within 1~10 nT. The plane of the magnetic field lines (MFLs) is mostly vertical to the equatorial plane, with the radius of curvature (Rc) of the MFLs being directed earthward and the binormal (perpendicular to the curvature and magnetic field direction) being directed azimuthally westward. The curvature radius of MFLs reaches a minimum, $R_{c,\min}$, at the CS center and is larger than the corresponding local half thickness of the neutral sheet, h. Statistically, it is found that the overall surface of the CS, with the normal pointing basically along the south-north direction, can be approximated to be a plane parallel to equatorial plane, although the local CS may be flapping and is frequently tilted to the equatorial plane. The tilted CS (normal inclined to the equatorial plane) is apt to be observed near both flanks and is mainly associated with the slippage of magnetic flux tubes. It is statistically verified that the minimum curvature radius, $R_{c,\min}$, half thickness of neutral sheet, h, and the slipping angle of MFLs, δ, in the CS satisfies $h = R_{c,\min}\cos\delta$. The current density, with a mean strength of 4–8 nA/m^2, basically flows azimuthally and tangentially to the surface of the CS, from dawn side to the dusk side. There is an obvious dawn-dusk asymmetry of CS, however. For magnetic local times (MLT) ~21:00–~01:00, the CS is relatively thinner; the minimum curvature radius of MFLs, $R_{c,\min}$ (0.6–1 R_E) and the half-thickness of neutral sheet, h (0.2–0.4 R_E), are relatively smaller, and B_z (3–5 nT) and the minimum magnetic field, $B_{\min}$ (5–7 nT), are weaker. It is also found that negative B_z has a higher probability of occurrence and the cross-tail current density j_Y is dominant (2–4 nA/m^2) in comparison to those values near both flanks. This implies that magnetic activity, e.g., magnetic reconnection and current disruption, could be triggered more frequently in CS with ~21:00–~01:00 MLT. Accordingly, if mapped to the region in the auroral ionosphere, it is expected that substorm onset would be optically observed with higher probability for ~21:00–~01:00 MLT, which is well in agreement with statistical observations of auroral substorm onset.

Citation: Rong, Z. J., W. X. Wan, C. Shen, X. Li, M. W. Dunlop, A. A. Petrukovich, T. L. Zhang, and E. Lucek (2011), Statistical survey on the magnetic structure in magnetotail current sheets, *J. Geophys. Res.*, *116*, A09218, doi:10.1029/2011JA016489.

1. Introduction

[2] The Earth's magnetotail current sheet (CS) is part of a transition layer which separates the antiparallel lobe field lines [e.g., *Ness*, 1965, 1969; *Behannon*, 1970; *Speiser*, 1973]. It is an extremely dynamic region in the magnetosphere, where magnetic reconnection and plasma instabilities are likely to be triggered, so as to release the stored energy, and which assumedly powers the geomagnetic storm/substorms process [e.g., *Baker et al.*, 1996; *Baumjohann et al.*,

[1]Beijing National Observatory of Space Environment, Institute of Geology and Geophysics, Chinese Academy of Sciences, Beijing, China.
[2]State Key Laboratory of Space Weather, Center for Space Science and Applied Research, Chinese Academy of Sciences, Beijing, China.
[3]Laboratory for Atmosphere and Space Physics and Department of Aerospace and Engineering Sciences, University of Colorado at Boulder, Boulder, Colorado, USA.
[4]Rutherford Appleton Laboratory, Didcot, UK.
[5]Space Research Institute, Moscow, Russia.
[6]Department of Geophysics and Planetary Sciences, USTC, Hefei, China.
[7]Space Research Institute, Austrian Academy of Sciences, Graz, Austria.
[8]Blackett Laboratory, Imperial College London, London, UK.

0148-0227/11/2011JA016489

1999; *Miura*, 2001; *Lui*, 2003]. Therefore, the tail CS always draws much attention in magnetospheric investigations.

[3] The magnetic field, **B**, and its related spatial gradients, including magnetic field gradient ∇B, current density, via $\mu_0^{-1}\nabla \times \mathbf{B}$, and curvature of the magnetic field lines (MFLs) $(\mathbf{B}/B \cdot \nabla) \times (\mathbf{B}/B)$, are key physical parameters for studying the dynamics of magnetospheric regions, especially those associated with the tail current sheets. Unambiguous knowledge of the form of the magnetic field and its related parameters are crucial to study the 3-D geometric structure of MFLs, the triggering of macroinstabilities or microinstabilities and magnetic reconnection, the control of the motion of charged particles, and the evolution and dynamics of space plasmas. However, because of the inability of single-satellite or double-satellite formations to separate the spatial-temporal variation of magnetic field except in very special circumstances, the magnetic spatial gradients have not been directly obtained from the earlier observation, although attempts have been made with two spacecraft simultaneous measurements [e.g., *McComas et al.*, 1986; *Sergeev et al.*, 1993], serendipitously.

[4] To explore the dynamics of magnetosphere more deeply, the Cluster mission [*Escoubet et al.*, 2001] was launched in the summer of 2000 into a $4 \times 19.6\ R_E$ polar, inertial orbit. One main goal of the elaborate four-satellite mission is to investigate the dynamics of the near-Earth magnetotail. During the end of June to early November each year, the Cluster orbit traverses the tail CS between 15 and 19 R_E from the Northern Hemisphere to the Southern Hemisphere, around its apogee, and from dawn to dusk, so that the whole tail CS can be investigated fully. The four-point observations of Cluster tetrahedron can, in principle, access the 3-D spatial structure of the magnetic field, given particular temporal behavior and sampling, through the developed four-spacecraft data analysis methods [*Dunlop et al.*, 1988] such as the spatial gradient [*Harvey*, 1998; *Chanteur*, 1998] or current density [*Dunlop et al.*, 2002a], the motional properties of magnetic discontinuities [e.g., *Dunlop and Woodward*, 1998; *Schwartz*, 1998; *Dunlop et al.*, 2002b; *Shi et al.*, 2005, 2006], and the 3-D geometry structure of MFLs [*Shen et al.*, 2003, 2007, and references therein].

[5] Recently, on the basis of the magnetic geometric configurations revealed, the magnetotail CS can be divided into three different types [*Shen and Dunlop*, 2008], i.e., the normal CS [*Shen et al.*, 2003, 2007], the flattened CS [*Shen et al.*, 2008a], and the tilted CS [e.g., *Nakamura et al.*, 2006; *Petrukovich et al.*, 2006; *Runov et al.*, 2005, 2006; *Shen et al.*, 2008b; *Rong et al.*, 2010a]. For the normal CS, the normal direction is generally along the magnetic south-north direction, the B_y component of magnetic field is much smaller than the B_z component, and the curvature at the CS center is directed earthward. The flattened CS, containing a strong B_y component (as a guide field), has a magnetic spiral structure, wherein the spiral structure is of the left-handed type for $B_y > 0$ and of the right-handed type for $B_y < 0$. For the tilted CS, which is generally induced by the flapping motion of the CS [e.g., *Zhang et al.*, 2002, 2005; *Sergeev et al.*, 2003, 2004; *Runov et al.*, 2005], the normal direction obviously leans away from the vertical direction, but the slippage of the planes of MFLs usually preserves the same magnetic geometry structure as that of the normal CS in the plane of the MFLs.

[6] Using the magnetic field data [*Balogh et al.*, 2001; *Gloag et al.*, 2010] from the single satellite Cluster-3 (Samba) during 2001–2005, we have recently carried out a preliminary statistical survey on the magnetic field in the CS center [*Rong et al.*, 2010b]. However, besides the directly measured magnetic field, there are more magnetic field-related parameters such as curvature radius of MFLs, curvature direction, current density, and the half thickness of neutral sheet (NS), derived from Cluster's multipoint observations, which could be involved in the statistical study. It is also to be expected that the statistical study with more parameters could yield and exhibit more detailed properties for the dynamic CS.

[7] In order to continue previous studies [*Shen et al.*, 2003, 2007, 2008a, 2008b; *Rong et al.*, 2010a, 2010b], the present study, with the advantage of Cluster's multipoint observations, statistically surveys the distribution properties of magnetic field-related parameters in the CS center, including the magnetic vector, curvature of MFLs, current density, and the normal of the CS. To simplify the study and the external solar wind dynamic pressure, interplanetary magnetic field (IMF), as well as any substorm process (usually indicated by *AE* index), have not been considered.

[8] Geocentric solar magnetospheric (GSM) coordinates are assumed throughout the study. In addition, it is convenient to use spherical coordinates for the vector direction (θ, φ) in the frame of GSM. The coordinate θ $(0° \le \theta \le 180°)$ is the angle between the positive z axis and the vector direction and is referred to as the polar angle; the coordinate φ $(0° \le \varphi \le 360°)$ is the angle between the positive x axis and the line from the vector direction projected onto the XY plane and is referred to as the azimuth angle. For example, the dawn direction or $-Y$ direction is (90°, 270°), while the dusk direction or $+Y$ direction is (90°, 90°).

2. Typical CS Crossing

[9] Before the start of this statistical study, it is necessary to examine a typical CS crossing event with Cluster multipoint observations in order to introduce the relevant parameters that are involved in the statistical survey. In this section, with newly developed multipoint data analysis approaches [*Shen et al.*, 2003, 2007; *Shen and Dunlop*, 2008], one current sheet crossing event on 5 August 2001 that has been previously studied by *Shen et al.* [2008b] will be briefly reviewed.

[10] As shown in Figure 1, there is a crossing event of the current sheet observed by Cluster on 5 August 2001 around 17:42–17:47 UT. During this period, Cluster locates at ~19 R_E far away from Earth center and traverses the CS from the Northern Hemisphere to the Southern Hemisphere.

[11] Figure 1a shows the magnetic field and its three components at the mesocenter of Cluster tetrahedron, i.e., $\mathbf{B} = \frac{1}{4}\sum_{i=1}^{4} \mathbf{B}_i$. Figure 1b shows the variation of magnetic vector direction (θ_B, φ_B), where the polar angle and azimuthal angles of its position in GSM are $(\theta, \varphi) = (85°, 206°)$ as indicated by the horizontal green line and violet line, respectively. Figure 1c shows the curvature radius of MFLs, R_c. Figure 1d shows the curvature direction (θ_c, φ_c) of MFLs. Figure 1e

shows the normal of the osculating plane, or the binormal (θ_N, φ_N) of MFLs. Note that, as illustrated in Figure 2, the magnetic unit vector $\hat{b}(\hat{b} = \mathbf{B}/B)$, curvature $\rho_c(\rho_c = (\hat{b} \cdot \nabla)\hat{b})$, and the binormal $\hat{N}(\hat{N} = \hat{b} \times \rho_c/|\hat{b} \times \rho_c|)$ are orthogonal to each other [*Shen et al.*, 2003], constituting the local natural coordinates of MFLs. Figure 1f shows the spatial magnetic rotation rate $\mu_1^{1/2}$, $\mu_2^{1/2}$, $\mu_3^{1/2}$ of magnetic vector quantitatively, which are calculated by the magnetic rotation analysis (MRA) method [*Shen et al.*, 2007; *Shen and Dunlop*, 2008]. The maximum rotation rate, μ_1, the median rotation rate, μ_2, and the minimum rotation rate, μ_3, are the eigenvalues of the magnetic rotation tensor $S_{ij} = \partial_i b_l \partial_j b_l (i,j,l = 1,2,3)$, and the half thickness of the one-dimensional neutral sheet (NS) can be estimated as $h = \mu_{1\max}^{-1/2}$ [*Shen et al.*, 2007; *Rong et al.*, 2010a]. Accordingly, Figure 1g shows the eigenvectors $\hat{e}_1(\theta_{e1}, \varphi_{e1})$ of eigenvalue μ_1. Particularly, the $\hat{e}_1$ can be seen as the normal of CS, along which the magnetic vector rotates most severely [*Shen et al.*, 2007; *Shen and Dunlop*, 2008; *Shen et al.*, 2008a]. Figure 1h shows the strength, j_t, and three components (j_x,j_y,j_z) of the current density at GSM coordinates; Figure 1i shows the field-aligned angle, γ, which has been defined as $\gamma = \cos^{-1}\left(\frac{\mathbf{j}\cdot\mathbf{B}}{|jB|}\right)$.

[12] Obviously, at the center of CS where B_x component reverses its sign, the strength of magnetic field reaches the minimum ($B_{\min} \sim 2.9$ nT). The curvature radius of MFLs reaches the minimum ($R_{c\ \min} \sim 0.28\ R_E$) at the CS center with the curvature direction (89°, 18°) pointing earthward and binormal (102°, 107°) pointing duskward, manifesting the 3-D geometry structure of MFLs in this CS; the magnetic vector rotates most severely in the CS, and the rotation rate reaches the maximum at CS center. Within this CS, μ_1 is much larger than μ_2 and μ_3, which implies that this CS is approximately a 1-D sheet, and the half thickness of the one-dimensional NS could be estimated as $h = \mu_{1\max}^{-1/2} \approx (1.8\pi/R_E)^{-1} \approx 1130$ km. The normal of CS as determined by $\hat{e}_1$ is (42°, 287°), which demonstrates that the CS is tilted. The current density with average strength being $\langle j \rangle \sim 2.8\ n\text{A/m}^2$ enhances in the CS, where $j_y \sim 2.1\ \text{nA/m}^2$, $j_z \sim 1.6\ \text{nA/m}^2$. At the CS center, the field-aligned angle reaches $\gamma \sim 44°$, indicating that the current density is more field aligned there relative to elsewhere.

3. Statistical Study

3.1. Selection and Preparation of Data

[13] The previous application of multipoint analysis methods [*Shen et al.*, 2003, 2007, and references therein] has demonstrated that the validities of these methods are mainly dependent on the assumption of linear variation of magnetic field within the Cluster tetrahedron, and the calculation error can be estimated as the order of L/D (L is the size of the Cluster tetrahedron, and D is the typical spatial scale of the magnetic structures). Therefore, to try to reduce the multipoint calculation errors originating from the linear assumption [*Chanteur*, 1998], we have adopted the 4 s magnetic field data [*Balogh et al.*, 2001; *Gloag et al.*, 2010] of four Cluster spacecraft during the years 2001, 2003, and 2004, as the characteristic size of the Cluster tetrahedron during magnetotail seasons in these years (less than 1600 km) is comparable to or less than the nominal CS thickness. We verify the validities in section 3.8.

[14] We have applied the multipoint analysis methods [*Shen et al.*, 2003, 2007, and references therein] to the magnetic field data of Cluster for the years 2001, 2003, and 2004 and have obtained the data set of magnetic-related parameters such as magnetic field, magnetic curvature, magnetic gradient, magnetic vector rotation rate, and current density at the mesocenter of the Cluster tetrahedron.

[15] To determine the tail CS crossing unambiguously, the criteria $B_x(t_i) \cdot B_x(t_{i+1}) < 0$ (where, t_i, t_{i+1} are the two successive measurements), combined with the lower strength of the magnetic field (<100 nT) and the nightside location of Cluster ($90° < \varphi < 270°$), have been used together in the first instance. With this procedure, the regions where the B_x also reverses around both polar cusps and the dayside CS can be excluded because of the stronger magnetic strength (hundreds of nT). Second, the visual inspection of the low plasma temperature ($<10 \times 10^6$ K), high density (>1 cm^3), and the tailward plasma velocity ($V_x < -100$ km/s) near the flanks (June to earlier July and later October-November, etc.) excludes the crossings of the magnetosheath [*Lucek et al.*, 2005] and low-latitude boundary layer [*Fujmoto et al.*, 1998]. Then, applying the linear interpolation to the data set, the interpolated parameters when $B_x = 0$, i.e., CS center have been grouped correspondingly as the basis data set for this statistical study. According to these selecting criteria, in total there are 5992 CS crossing events obtained. The criteria obtain 1507 CS crossing events for 2001, 2785 events for 2003, and 1700 events for 2004. On the basis of the derived data set, we can statistically study the detailed distribution of magnetic structure at the CS center in detail.

[16] Figure 3 shows the projection of Cluster locations at the moment of CS crossings onto the *XY* plane (Figure 3a) and *YZ* plane (Figure 3b). It can be seen that the *Y* direction scale of CS on the downstream $0 < |X| < 20\ R_E$ is about $35\ R_E$ (Figure 3a). The obtained CS configuration is wavy (as in Figure 3b) and warps severely at both flanks; it warps down toward the negative z axis (June-July) near the dawn side and warps up toward the positive z axis (October-November) near the dusk side. As to the configuration of CS, controlling factors such as geodipole tilt angle and solar wind conditions have been noticed, and some empirical models have been formulated accordingly [e.g., *Fairfield*, 1980; *Tsyganenko et al.*, 1998; *Tsyganenko and Fairfield*, 2004]. Therefore, it should be noted that our obtained CS configuration is just a temporal superposition as the values of controlling factors at the different crossing moment are different. As a comparison, a calculated CS configuration with the same (x,y) coordinates of measurements has been shown in Figure 3b as the red dots on the basis of *Tsyganenko and Fairfield*'s [2004] model with geodipole tilt angle only being considered. It is clear, under the modulation of geodipole tilt angle, that the modeled CS basically reproduces the similar wavy configuration as we observed, though the modeled CS excurses upward a bit at the dawn side. On the basis of Cluster measurements, *Petrukovich et al.* [2005] gave a detailed analysis on CS configuration in comparison with models and argued that Tsyganenko and Fairfield's model is the better model to fit the actual observations. To study the shape of tail CS is not the main goal of this research, and we do not intend to discuss it any further here.

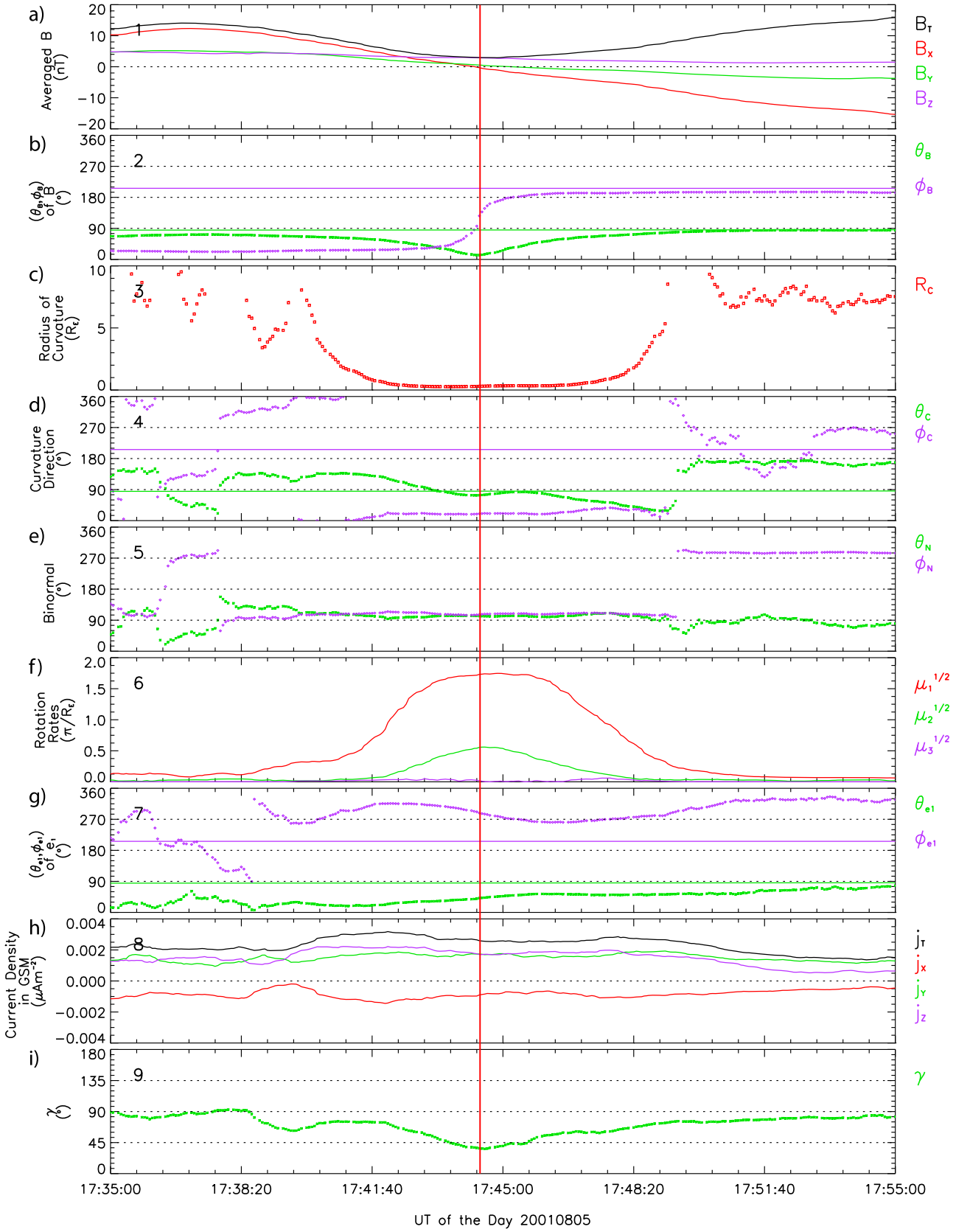

Figure 1. (a-i) The geometric structure of the current sheet during one Cluster crossing event on 5 August 2001 (modified from *Shen et al.* [2008b]).

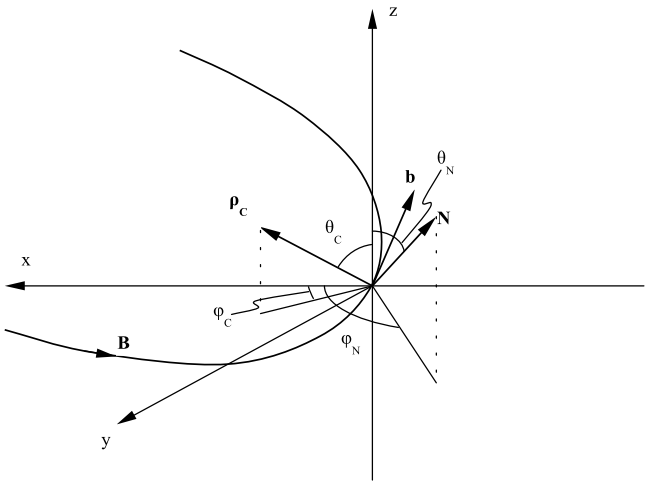

Figure 2. Illustration of the 3-D magnetic geometric structure with the relationship between the unit magnetic vector **b**, curvature vector $\boldsymbol{\rho}_c$, and the binormal vector **N** of the osculating plane of one magnetic field line in GSM coordinates (adapted from *Shen et al.* [2003]).

3.2. Distribution of Magnetic Field

[17] Here we first statistically investigate the distribution of magnetic field; part of the results are consistent with our previous study [*Rong et al.*, 2010b]. In Figure 4, the histogram distribution of the B_y, B_z, component and the minimum magnetic strength $B_{\min}$ ($B_{\min} = \sqrt{B_y^2 + B_z^2}$) are shown in Figures 4a, 4b, and 4c, respectively. The azimuthal distribution of averaged B_y, B_z, and B_{min} are shown in Figures 4d, 4e, and 4f, respectively.

[18] It is clear that the histogram distribution of the B_y component (Figure 4a) is basically symmetric about $B_y = 0$ nT and has higher probability to occur within $|B_y| < 5$ nT, which could be well approximated as the normal distribution [*Rong et al.*, 2010b], whereas the B_z component (Figure 4b) is mainly positive and distributes between 1~10 nT. Similarly, the minimum magnetic strength B_{min} also mainly distributes within 1~10 nT (Figure 4c). As to the azimuthal distribution, on average, B_z (Figure 4e) and $B_{\min}$ (Figure 4f) are stronger near both flanks (B_z, 7–15 nT; $B_{\min}$, 9–15 nT) but weaker (B_z, 3–5 nT; $B_{\min}$, 5–7 nT) within the azimuth scope ~140°–200°, i.e., the magnetic local times (MLT) ~21:00–~01:00, which suggests that the curvature radius of MFLs is smaller and tail CS is relatively thinner there [*Büchner and Zelenyi*,1989]. In contrast, on average, the B_y component is stronger and negative at both flank regions but weaker and positive around the midnight region (Figure 4d).

[19] However, this azimuthal distribution of B_y can be attributed to the seasonal modulation of geodipole tilt angle [*Petrukovich*, 2009]. On the basis of Geotail's measurements, *Petrukovich* [2009, p. 1343] statistically discovered that the B_y in CS is correlated with the geodipole tilt angle; that is, "…At midnight and pre-midnight local times B_y is positively correlated with tilt while dawn side plasma sheet B_y generally does not exhibit any tilt dependence, but within 15 R_E negative correlation with tilt was revealed…." As shown in Figure 5a, the B_y component in CS is consistently, positively correlated with geodipole tilt angle (negative sign) at the premidnight region (October-November) but is negatively correlated with geodipole tilt angle (positive sign) at the postmidnight region (July-June). Therefore, as shown by Figure 5b, it suggests that the orientation of magnetic vector in CS could be warped by the large-scale shape of CS and modulated by the seasonal effect of geodipole tilt angle [*Tsyganenko and Fairfield*, 2004].

3.3. Three-Dimensional Geometry Structure of MFLs

[20] With Cluster multipoint measurements, cases studies of the geometric structure of MFLs in tail CS have been carried out previously [e.g., *Runov et al.*, 2003, 2005; *Shen et al.*, 2003, 2007, 2008a, 2008b]. However, to reveal the global distribution characteristics of the MFLs' structure, it is necessary to survey the MFLs' geometric structure at tail CS center statistically.

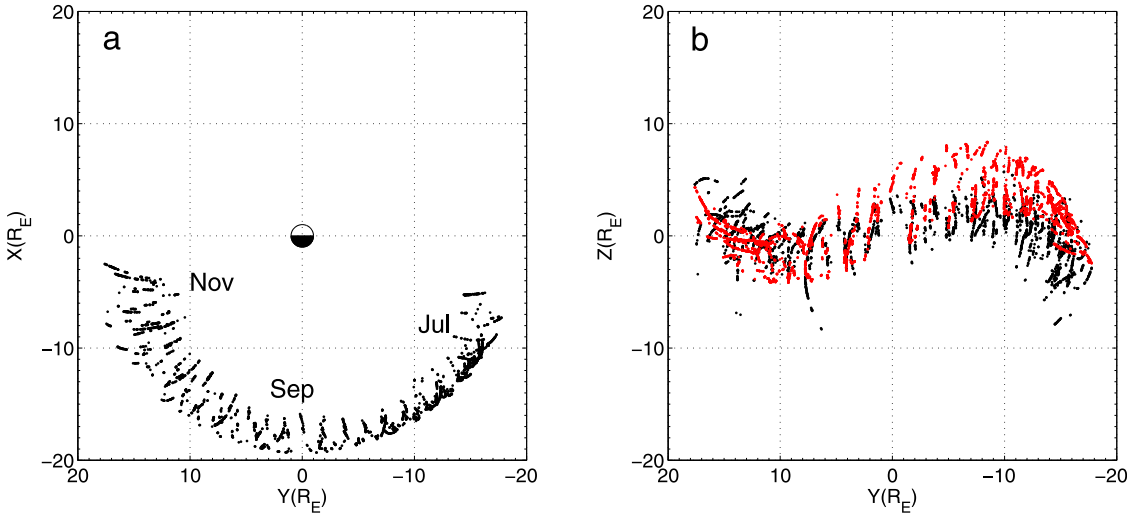

Figure 3. The observed locations of CS center projected onto (a) the *XY* plane and (b) the *YZ* plane as the black dots. In contrast, the locations of the CS calculated from *Tsyganenko and Fairfield*'s [2004] model are also shown as the red dots in Figure 3b (see text for details).

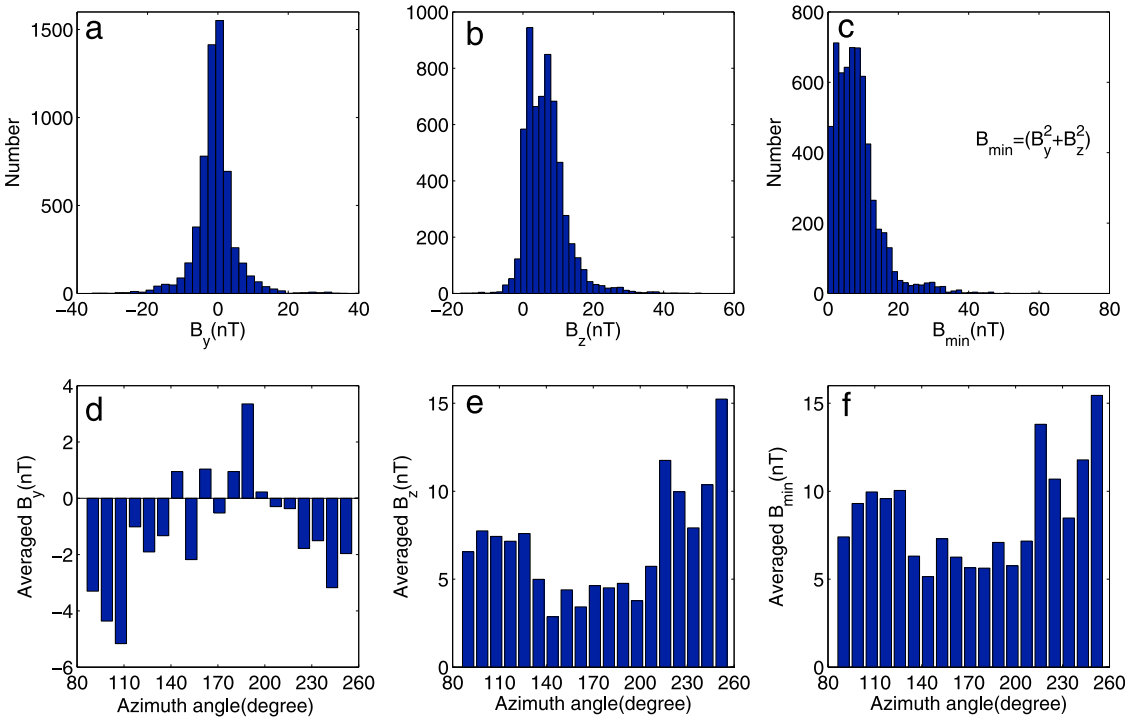

Figure 4. Histogram of (a) B_y, (b) B_z, and (c) $B_{\min}$ in the CS center and the corresponding azimuth distribution of averaged (d) B_y, (e) B_z, and (f) $B_{\min}$.

[21] On the basis of the derived data set, Figure 6 shows the angle histogram of the MFLs' curvature direction in terms of azimuth angle (Figure 6b) and polar angle (Figure 6d) and that of MFLs' binormal direction for the azimuth angle (Figure 6c) and polar angle (Figure 6e). It is clear from the histogram of azimuth angle that, at the CS center, the curvature of MFLs $\boldsymbol{\rho}_c$ mostly directs earthward and the binormal $\hat{N}$ directs duskward; meanwhile, both polar angles mainly distribute around 90°. It implies that the magnetic vector, $\hat{b}$, i.e., $\mathbf{B}/B$, at the CS center is mostly along the z axis if noting the orthogonal relationship between $\hat{b}$, $\boldsymbol{\rho}_c$ and $\hat{N}$, i.e., $\hat{N} = \hat{b} \times \boldsymbol{\rho}_c / |\hat{b} \times \boldsymbol{\rho}_c|$ [*Shen et al.*, 2003, 2007]. Actually, we can define the tilt angle of MFLs as $a = \arccos(\hat{b} \cdot \hat{z})$ to describe the deviation of magnetic vector $\hat{b}$ from the z axis (unit vector $\hat{z}(0,0,1)$). Being consistent with the angle histogram of curvature and the binormal, the histogram of MFLs' tilt angle (Figure 6a) demonstrates that the magnetic vector $\hat{b}$ is mostly along the z axis. These histograms of Figure 6 clearly show that the osculating planes of MFLs at tail CS center are mostly perpendicular to the equatorial plane.

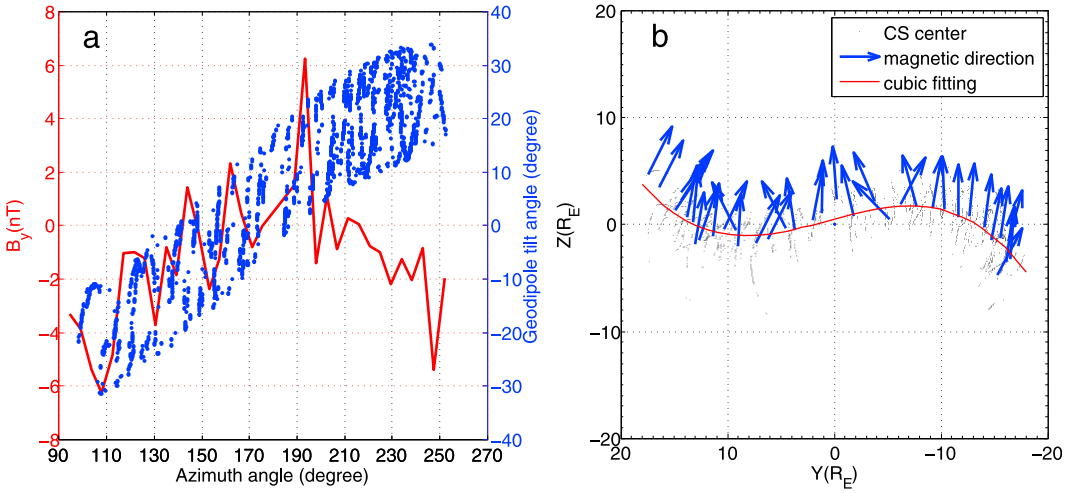

Figure 5. (a) Average distribution of B_y component (blue dots) and geodipole tilt angle (red line). (b) Average magnetic field direction (blue arrows) in the CS center with polynomial cubic fitting (red line) of CS configuration.

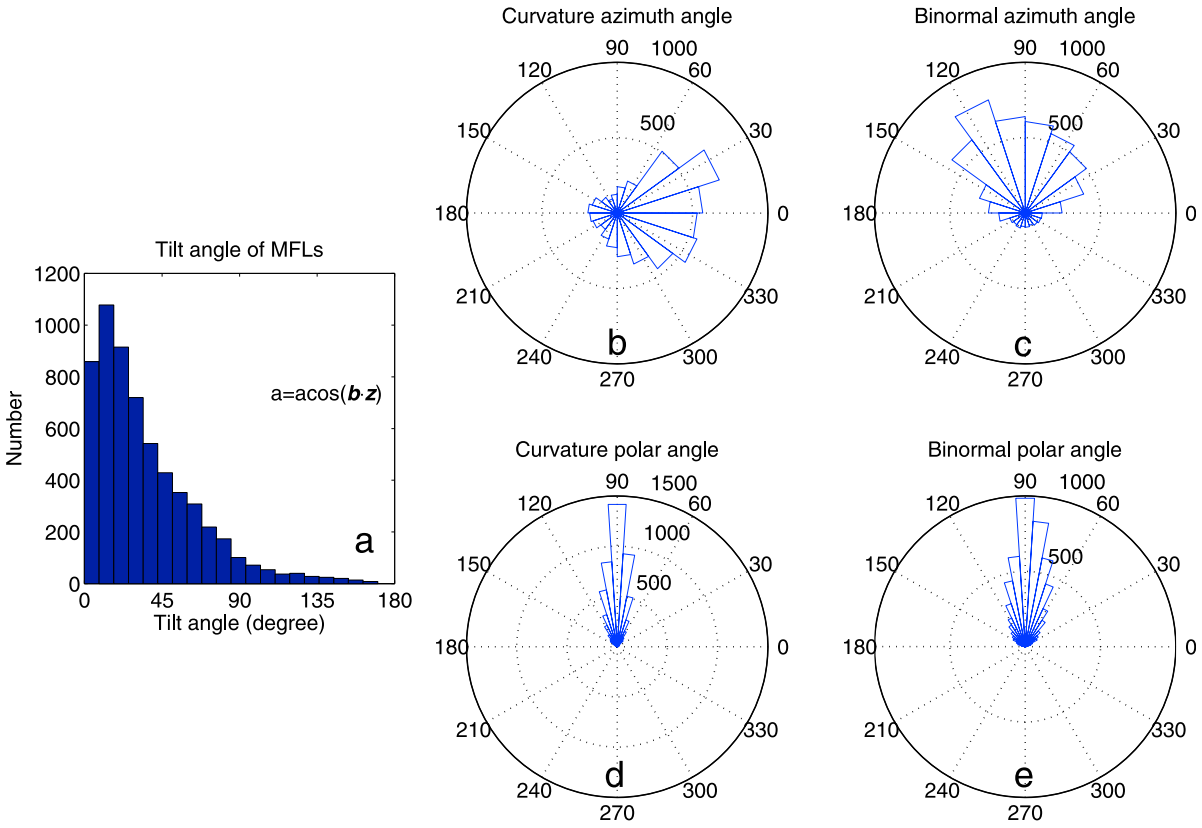

Figure 6. (a) Histogram of the MFLs' tilt angle. Angle histogram of the curvature direction and binormal direction of MFLs in terms of (b, c) azimuth angle and (d, e) polar angle.

[22] Accordingly, Figure 7 shows the averaged spatial orientation of curvature direction and the binormal that projected onto the *XY* plane (Figure 7a) and *YZ* plane (Figure 7b). It is obvious that, in the whole azimuth scale, the curvatures of MFLs are on average directed earthward, and the binormal are, on average, directed duskward. At dawn side ($Y < 0$), the curvature direction has a duskward component, while the binormal has a tailward component; on the dusk side ($Y > 0$); the curvature direction has a dawnward component, while the binormal has an earthward component, which implies that the configuration of MFLs in the magnetotail is flaring [e.g., *Fairfield*, 1979]. On average, the directions of curvature and binormal are in the *XY* plane, but near the dusk flank region ($Y > 10\ R_E$) the curvature has

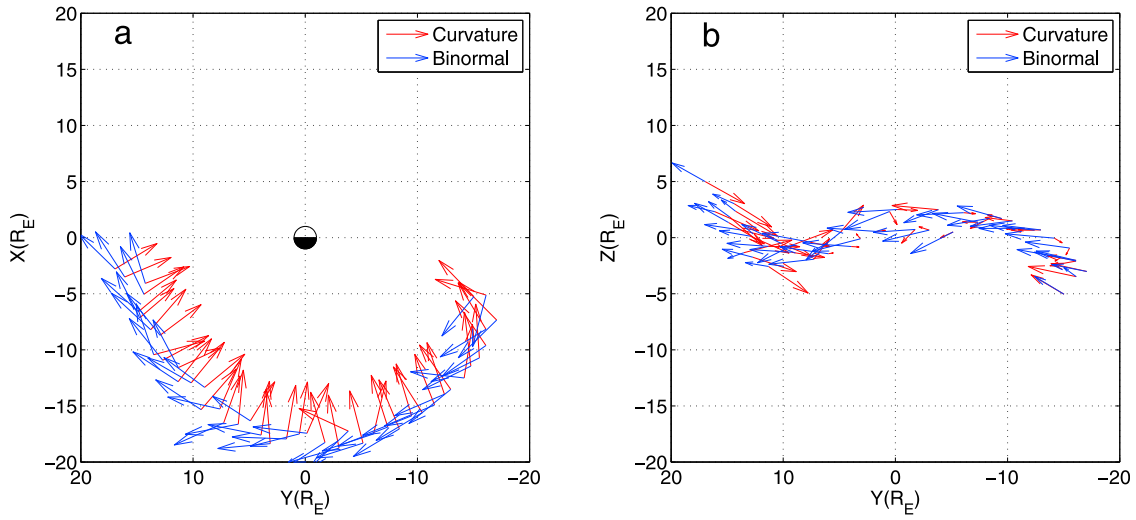

Figure 7. The spatial averaged curvature direction (red arrows) and binormal (blue arrows) of MFLs at the CS center as projected onto (a) the *XY* plane and (b) the *YZ* plane.

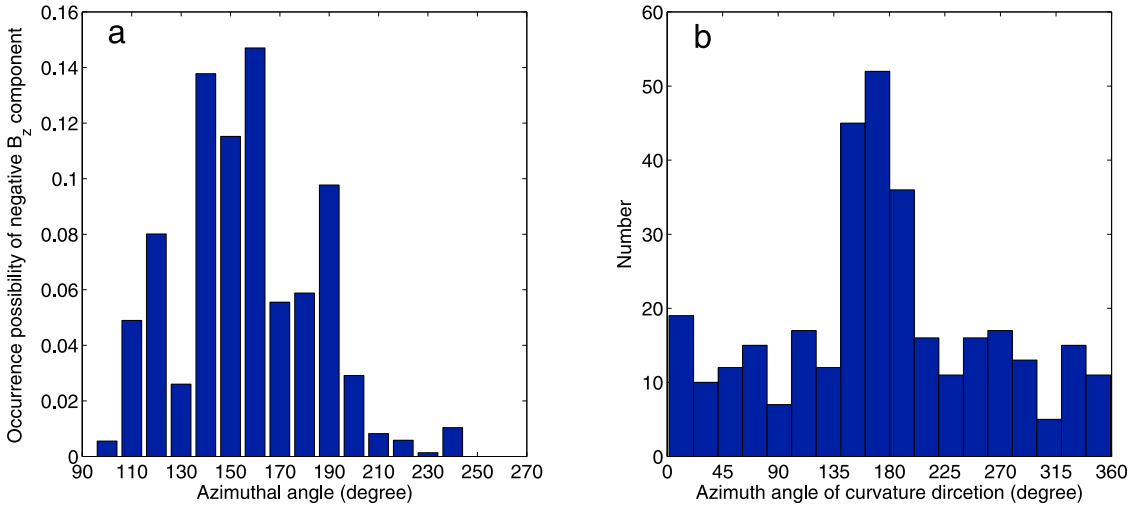

Figure 8. (a) The occurrence possibility of negative B_z component in CS center. (b) Histogram of the azimuth angle of curvature direction associated with negative B_z.

an obvious southward component. It may suggest that the magnetic field configuration near the dusk flank is more inclined to be twisted.

3.4. Negative B_z Component

[23] The B_z component at CS center is basically assumed northward as the magnetic flux emanating from the south polar region would traverse tail CS and converge into the north polar region. However, because of the crossings of magnetic reconnection [e.g., *Øieroset et al.*, 2001; *Runov et al.*, 2003], plasmoid/flux rope [e.g., *Hughes and Sibeck*, 1987; *Slavin et al.*, 1995], or magnetic turbulence induced by current disruption [e.g., *Lui*, 1996], negative B_z values can also be observed in the CS. Therefore, to some extent, regions of negative B_z in tail CS can indicate the regions where magnetic activities occur, and it is meaningful to study the distribution of negative B_z as well as its associated magnetic structure.

[24] From the data set, we obtain 329 crossing cases with negative B_z component at CS center. To check the distribution properties of the negative B_z component, it is helpful to define the local occurrence probability in one bin of azimuth angle as the ratio of the CS crossing number with negative B_z to the total CS crossing number in that bin. The conception of occurrence probability also can be applied similarly to the other parameters in sections 3.6 and 3.8. As shown in Figure 8a, the negative B_z has higher occurrence probability within the azimuth scope ~140°–200°, i.e., the magnetic local times ~21:00–~01:00, which is consistent with previous studies [*Fairfield*, 1986; *Rong et al.*, 2010b].

[25] Meanwhile, it is worth checking the geometric structure of MFLs associated with those negative B_z. In Figure 8b, the histogram shows clearly that the azimuth angle of curvature direction of MFLs associated with negative B_z are mostly distributed around 180°, so that the curvature is mostly directed tailward. It exhibits the consistency with the standard macroscopic picture of the X-type magnetic reconnection where the curvature direction of MFLs associated with negative B_z are expected to direct tailward. Therefore, our statistical results may suggest that the negative B_z at CS center are mostly a result of the magnetic reconnection process which can occur in the regions with $X > -20\ R_E$. If we interpret the negative B_z as the sign of magnetic reconnection, it also suggests that the magnetic reconnection is more inclined to be triggered in the CS regions with MLT being ~21:00–01:00.

3.5. Normal of Current Sheet

[26] The eigendirection of the maximum magnetic rotate rate, $\hat{e}_1$, could be seen as the proxy of normal direction of CS, $\hat{n}$ [*Shen et al.*, 2007; *Shen and Dunlop*, 2008; *Shen et al.*, 2008a, 2008b]. Therefore, with the knowledge of $\hat{e}_1$, the large-scale orientation of CS surface can be investigated.

[27] Figure 9 (top to bottom) shows the average azimuth histogram for the normal's three components in GSM, i.e., n_x, n_y, and n_z. It shows that, on the whole, the positive n_z dominates the CS normal, n_x is minor and negative always azimuthally, and n_y could be ignorable by comparison. Hence, it demonstrates that the surface of CS could approximately be a plane with the normal directing basically along the z axis, and such type of plane exhibits a bit of deviation from the X-Y plane as the normal tilting antisunward (indicated by the negative n_x). Near both flanks the CS is warped severely as indicated by the relative minor n_z there.

[28] The negative n_x that appeared on average throughout the whole dawn-dusk scale is independent of the seasonal variation of geodipole tilt angle (note that the tilt angle is positive at the dawn side but negative at the dusk side; see Figure 5a), which would yield an inconsistency with the empirical CS models [e.g., *Tsyganenko and Fairfield*, 2004]. When the geodipole tilt angle is positive, the displacement of CS to the equatorial plane in Tsyganenko and Fairfield's model is expected to increase up to a constant in the far tail, which would yield a noticeably positive n_x in the near-Earth tail, e.g., $X = -10$~$-20\ R_E$. True reasons to explain the tailward tilting of CS are still unknown.

[29] Comparing n_x and n_z, although the n_y component can be ignored, the negative sign of n_y shown at the dawn and dusk sides would suggest that the surface of the CS could be modulated by the seasonal variation of geodipole tilt angle.

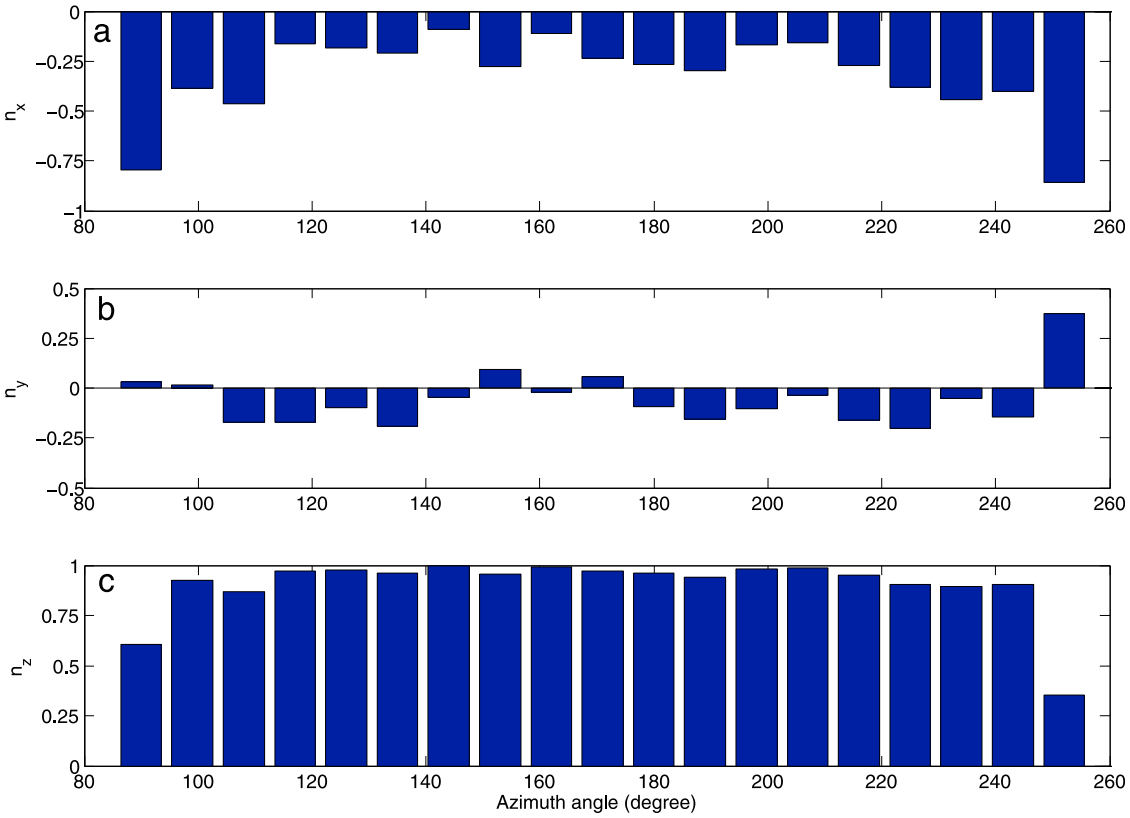

Figure 9. Average azimuth distribution for the three components of normal vector **n** in GSM: (a) n_x, (b) n_y, and (c) n_z.

On the dawn (dusk) side, when tilt angle is positive (negative), the CS would be induced, forming an arch-like (reversal arch-like) configuration in the *YZ* plane [*Tsyganenko and Fairfield*, 2004], which would yield the normal tilting dawnward at the dawn (dusk) side.

3.6. Tilted CS

[30] Frequently, the normal of the CS evidently deviates from the *z* axis and leans to the equatorial plane, forming one tilted CS [e.g., *Petrukovich et al.*, 2006; *Shen et al.*, 2008b]. Generally, the tilted CS can be locally induced by the flapping motion of CS that is launched as kink-like flapping waves from midnight propagating toward the flanks [e.g., *Zhang et al.*, 2002; *Sergeev et al.*, 2003, 2004; *Runov et al.*, 2005]. Here, with the data set of CS normal, it is meaningful to statistically investigate the distribution of tilted CS.

[31] For simplicity, we define CS with the polar angle of normal direction $45° \le \theta_{e1} \le 135°$ to be a tilted CS. With this criterion, 3662 events are obtained for tilted CS, which takes up 61% of the total CS crossings, which suggests that the tilted CS is not a occasional case but occurs frequently.

[32] Figure 10 shows the histogram of occurrence distribution of the tilted CS. It is clear, within the azimuth angle ~140°–~200°, that the occurrence possibility of tilted CS is relatively lower while it increases toward both flanks, which indicates that the tilted CS is apt to be observed toward both flanks. Thus, it suggests that the CS is warped and twisting severely near the flanks; on the other hand, the transient waves or magnetic fluctuations, e.g., flapping motion, would be more active toward both flanks.

[33] *Petrukovich et al.* [2006] suggested that the local warped CS would probably result in two kinds of configuration of MFLs, i.e., the "slip type" and the "bend type," as sketched in Figure 11 (left). The detailed case studies demonstrate that the magnetic configuration in tilted CS is the slip type; that is, magnetic flux tubes in tilted CS are

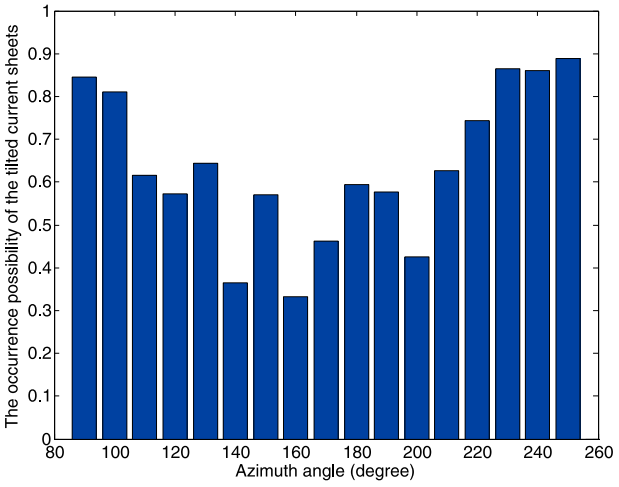

Figure 10. Azimuth histogram distribution of the occurrence possibility of tilted CS.

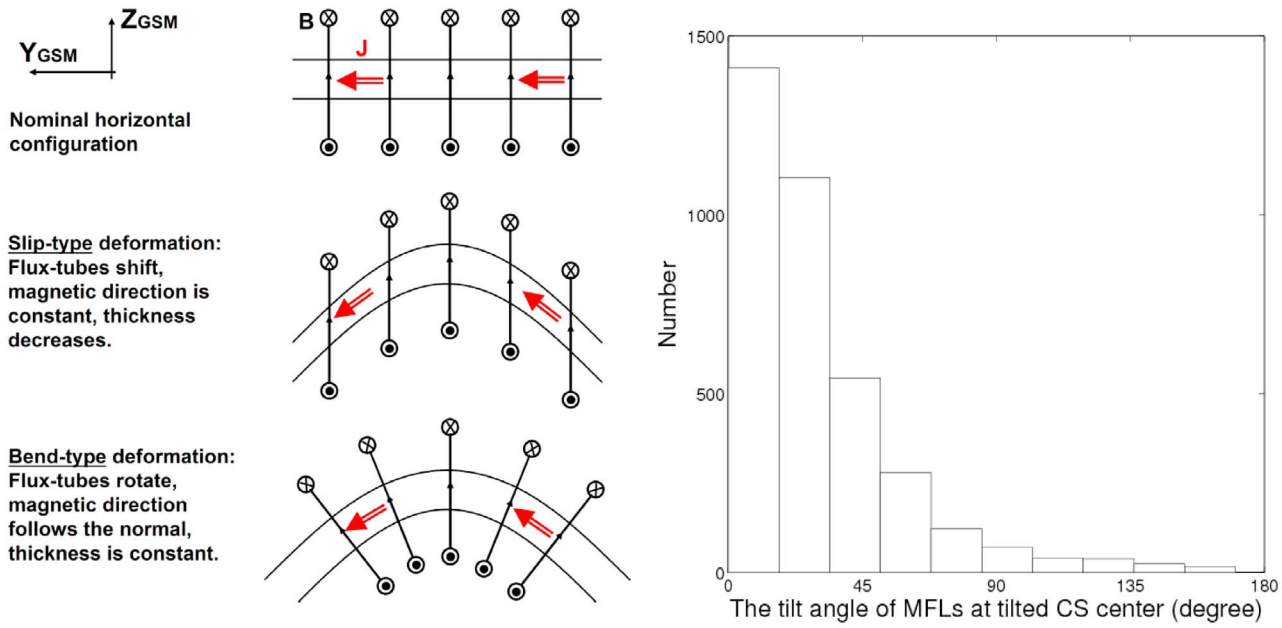

Figure 11. (left) Cartoon of the possible magnetic configuration in the deformed current sheet [see *Petrukovich et al.*, 2006]. (right) Histogram of tilt angle of MFLs in tilted current sheets.

basically slipped from each other to some extent with a dominant B_z component [*Petrukovich et al.*, 2006; *Shen et al.*, 2008b]. Preliminary statistical studies (with 360 cases of Cluster during 2001 and 2004) found that the tilted CS usually has B_y either within 2 nT or smaller than B_z [*Petrukovich*, 2009].

[34] As a continuation of the study, we check the magnetic configuration in the tilted CS from the statistical perspective. Figure 11 (right) shows the histogram of the tilt angle of MFLs for the selected tilted CS. Obviously, the tilt angle of MFLs in tilted CS is mostly (2918 events out of the total 3662 events) less than 45°, which means that most of the MFL planes (80%) in tilted CS are perpendicular to the equatorial plane. Thus, our result is consistent with the slip type of MFL configuration in tilted CS as observed in the previous studies [*Petrukovich et al.*, 2006; *Petrukovich*, 2009; *Shen et al.*, 2008b].

3.7. Classification of Current Sheets

[35] Previously, we have statistically studied the structure of the magnetic field and the normal direction of the CS; thus, it is necessary to classify the CS with this knowledge as a summary. We may first classify the CS only on the basis of the tilt angle of MFLs into three types: the first type with tilt angle $a < 45°$, the second type with $45° \le a \le 90°$, and the third type with $a > 90°$. In first type, the B_z component is positive and dominant in CS. By comparison, in the second type, the B_y component is dominant and stronger than the positive B_z in the CS. For the third type, the B_z component is negative and may induced by the magnetic reconnection or flux ropes, etc. As shown in Figure 12a, the gross classification indicates that the first type is the most frequent to occur in tail CS, which occurs 71% of the time and implies that the B_z component is mostly dominant. The second type occurs 23% of the time with the proportion being one third of the first type, which is consistent with our previous results [*Rong et al.*, 2010b]. The third type makes up 5% of the total, which means that the CS with negative B_z is an accidental event, at least for $X > -19\ R_E$.

[36] *Shen and Dunlop* [2008] suggested that the magnetotail CS could be divided into three types: normal CS, flattened CS, and tilted CS on the basis of the different magnetic geometric structure and the local CS orientation. For the normal CS [*Shen et al.*, 2003, 2007], the normal is generally along the south-north direction with dominant B_z component embedding it. The flattened CS [*Shen et al.*, 2008a], with normal also basically along the south-north direction, contains a strong B_y component forming a magnetic spiral structure. For the tilted CS [e.g., *Zhang et al.*, 2002, 2005; *Sergeev et al.*, 2003, 2004; *Runov et al.*, 2005, *Petrukovich et al.*, 2006; *Shen et al.*, 2008b], the normal evidently deviates from the z axis, and the magnetic flux tubes are basically slipped with dominant B_z component.

[37] To quantify the three CS types proposed by *Shen and Dunlop* [2008], we would define the normal CS as the CS with the polar angle of normal $0° \le \theta_{e1} < 45°$, $135° < \theta_{e1} \le 180°$ and tilt angle $a < 45°$; define the flattened CS as the CS with the same range of normal's polar angle but with tilt angle $45° \le a \le 90°$; and define the tilted-slipping CS as the CS with the polar angle of normal $45° \le \theta_{e1} \le 135°$ and tilt angle $a < 45°$ (to differentiate the tilted CS, we defined it solely with $45° \le \theta_{e1} \le 135°$ in section 3.6). Then the remaining events that are not classified would be attributed to the type of the others. With such quantitative definition, Figure 12b shows that the proportion of tilted-slipping CS is 49%, nearly half of the total amount, while the proportion of normal CS is 22%. The total proportion of both is 71%, which is equal to the first type as indicated by Figure 12a. The flattened CS is 14% of the total amount, while the other type is 15% of the total.

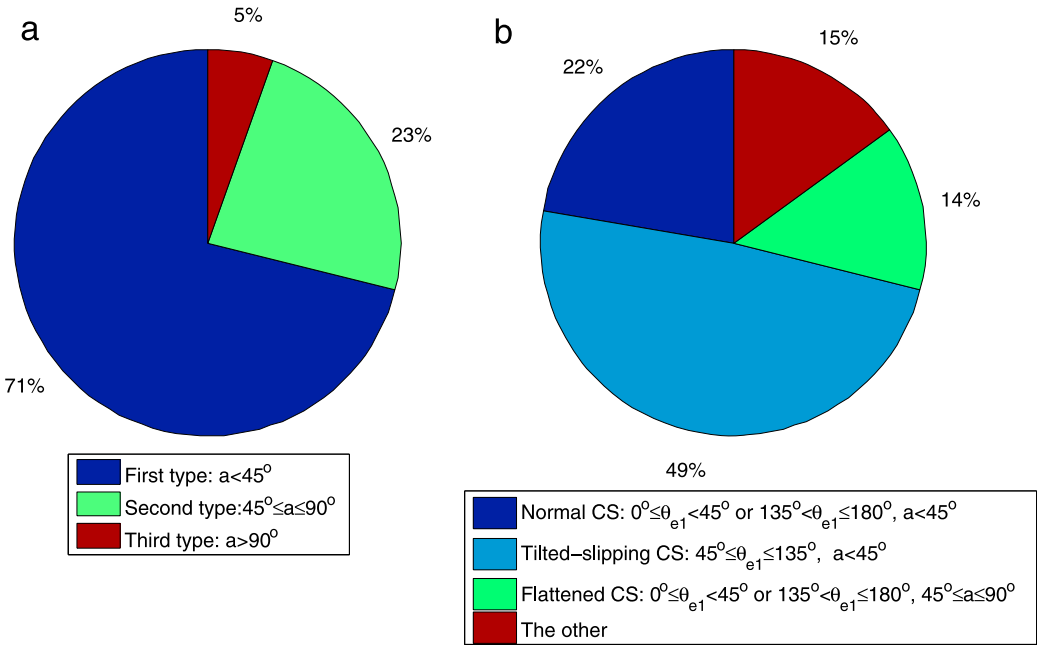

Figure 12. Pie plots to show the proportion of CS types (a) based only on the tilt angle of MFLs and (b) based on the tilt angle and CS normal together. See the text for details.

3.8. Curvature Radius and Half Thickness of the Neutral Sheet

[38] The minimum curvature radius, $R_{c,\min}$, and half thickness of NS, h, are the key parameters to determine the characteristic scale of the CS and the adiabatic nature of charged particles [e.g., *Büchner and Zelenyi*, 1987, 1989; *Shen et al.* 2008a]. Therefore, it is meaningful to check their distributions properties.

[39] According to previous work [*Shen et al.*, 2007], the neutral sheet (NS) is defined as a region in the current sheet where $B \le \sqrt{2}B_{\min}$, where $B_{\min}$ is the minimum strength of the magnetic field in the CS center. In particular, if the maximum rotation rate, μ_1, is much larger than the middle and minimum rotation rates, μ_2 and μ_3, the sheet can be well approximated as a 1-D sheet, so that the 1-D half thickness of the NS can be estimated as $h = \mu_1^{-1/2}$ [e.g., *Shen et al.*, 2007; *Rong et al.*, 2010a]. The azimuth histogram of the ratio $(\mu_1/\mu_2)^{1/2}$ is shown in Figure 13c. It clearly shows that $\mu_1 \gg \mu_2$, μ_3, as $(\mu_1/\mu_2)^{1/2} \sim 5$ uniformly in the azimuth direction, which implies that the current sheet could be well approximately as the 1-D sheet. Therefore, the half thickness of the NS could be well estimated as $h = \mu_1^{-1/2}$.

[40] Figures 13a and 13b show the azimuth histogram of the minimum curvature radius of MFLs, $R_{c,\min}$, and the half thickness of the NS, h, respectively. It shows obviously, that the minimum curvature radius, $R_{c,\min}(1/\rho_{c,\max})$, is on average larger than the half thickness of the NS, h, at the given azimuth bin. It is also interesting to note that in the range of azimuth angle ~140°–~200°, i.e., MLT being ~21:00–01:00, $R_{c,\min}$(0.6–1 R_E) and h(0.2–0.4 R_E) are relatively smaller, while near both flanks $R_{c,\min}$(3–5 R_E) and h(0.7–1.6 R_E) are relatively larger, which suggests that the current sheet is usually thinner with MLT ~21:00–01:00 but thicker near both flanks. Such thickness distribution is in agreement with the earlier studies [e.g., *Kaufmann et al.*, 2001], and it is also consistent with that inferred from the B_z distribution in section 3.2.

[41] In addition, the distribution of $R_{c,\min}$ and h verifies that the typical size of the Cluster tetrahedron during these seasons (less than 1600 km, ~0.25 R_E) is indeed grossly less than the average minimum curvature radius of MFLs, $R_{c,\min}$, and the half-thickness of the NS in the whole azimuth direction (certainly, in some cases, e.g., substorm growth phase, the half thickness of the NS could reach several hundred kilometers). Therefore, it is reasonable to believe the validity of our analysis methods for the statistical survey.

[42] If we defined the CS with the half thickness of the NS being less than 1000 km to be the thin CS, we can further check the distribution of the thin CS, in particular. With this definition, we obtain 1803 crossing events of thin CS from the total 5992 CS crossing events; thus, the occurrence possibility of the thin CS is 0.3 overall. Figure 14 shows the azimuth histogram distribution of the occurrence possibility of thin CS. It clear from Figure 14 that there is a higher probability of occurrence of thin CS within the range of azimuth angle ~140°–~200°, where the CS is usually thinner.

[43] A previous case study [*Shen et al.*, 2008b] and theoretic analysis [*Rong et al.*, 2010a] demonstrate that the minimum curvature radius, $R_{c,\min}$, and the half thickness of NS, h, are geometrically correlated as $h = R_{c,\min} \cos\delta$, where δ is the slipping angle of MFLs that is the angle between the normal of CS($\hat{e}_1$) and the plane of MFLs. Here, with the abundant data set of CS crossings, it is meaningful to verify this geometrical relation from the statistical perspective. Continuing the definition from previous studies [e.g., *Shen et al.*, 2008b; *Rong et al.*, 2010a], here the slipping angle δ of MFLs in CS is the angle between magnetic vector $\hat{b}$ and the normal of CS, $\hat{n}$, i.e., $\delta = \arccos(|\hat{b} \cdot \hat{n}|)$.

[44] As shown in Figure 15a, the minimum curvature radius, $R_{c,\min}$, is generally larger than the corresponding

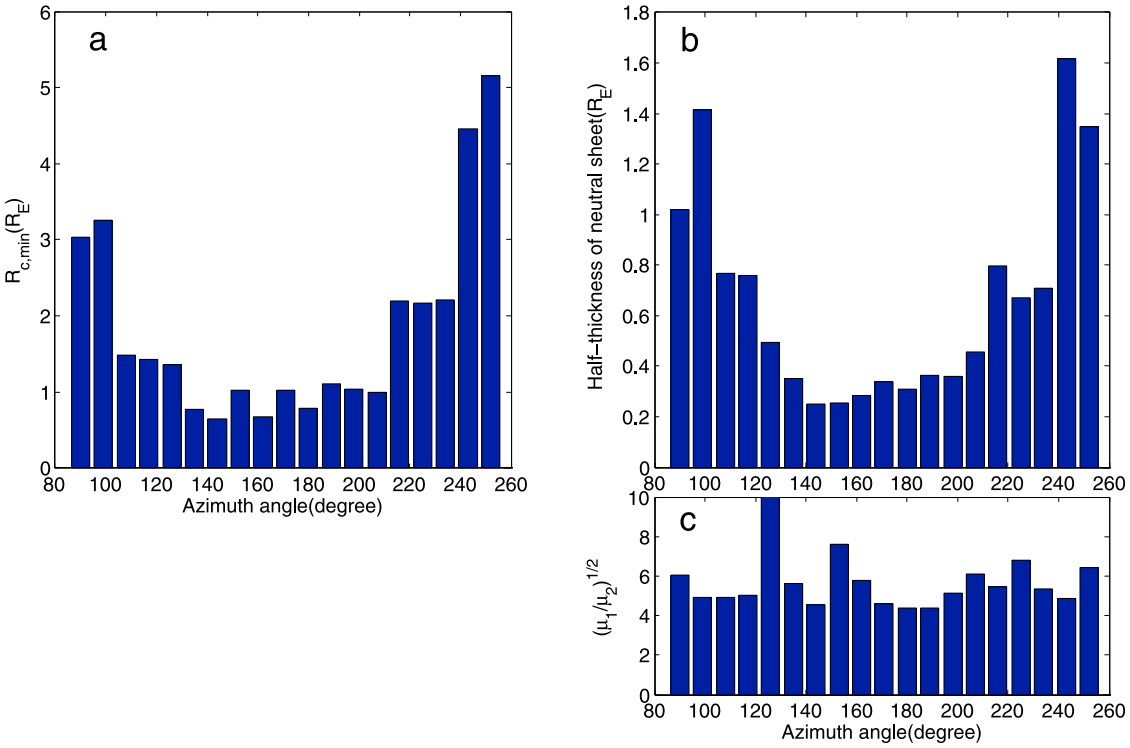

Figure 13. Azimuth histograms of (a) the minimum curvature radius, $R_{c,\min}$, (b) the half thickness of NS, h, and (c) the ratio of $(\mu_1/\mu_2)^{1/2}$.

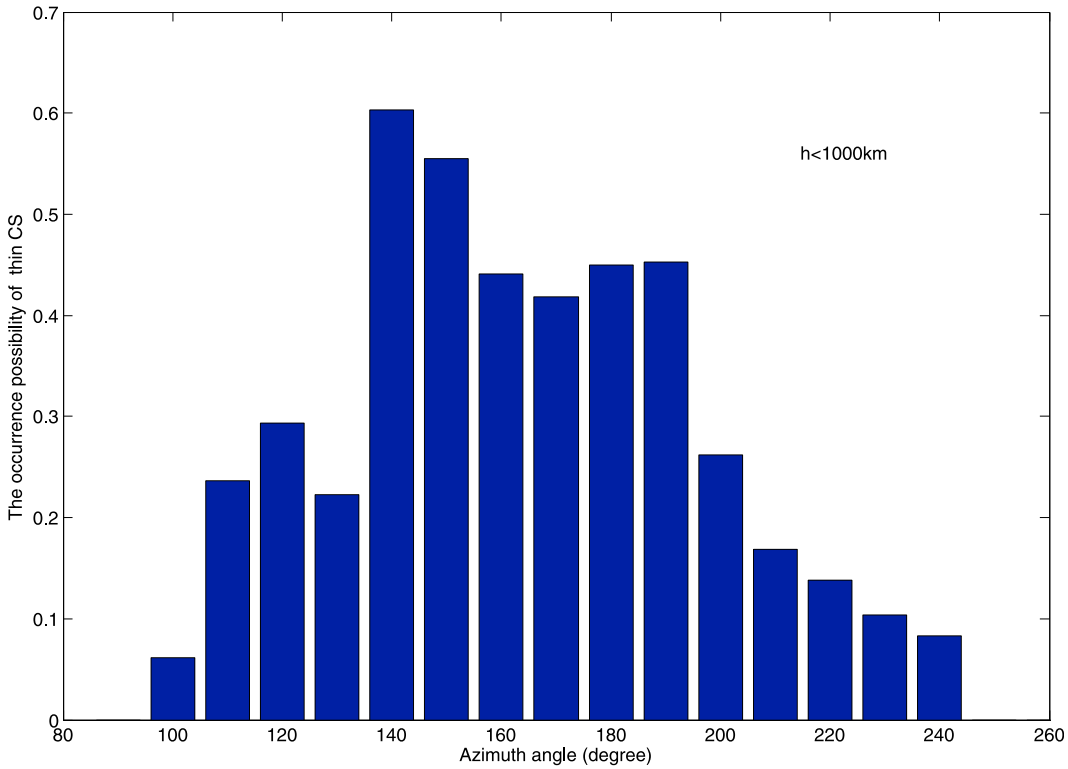

Figure 14. Azimuth histogram distribution of the occurrence possibility of thin CS.

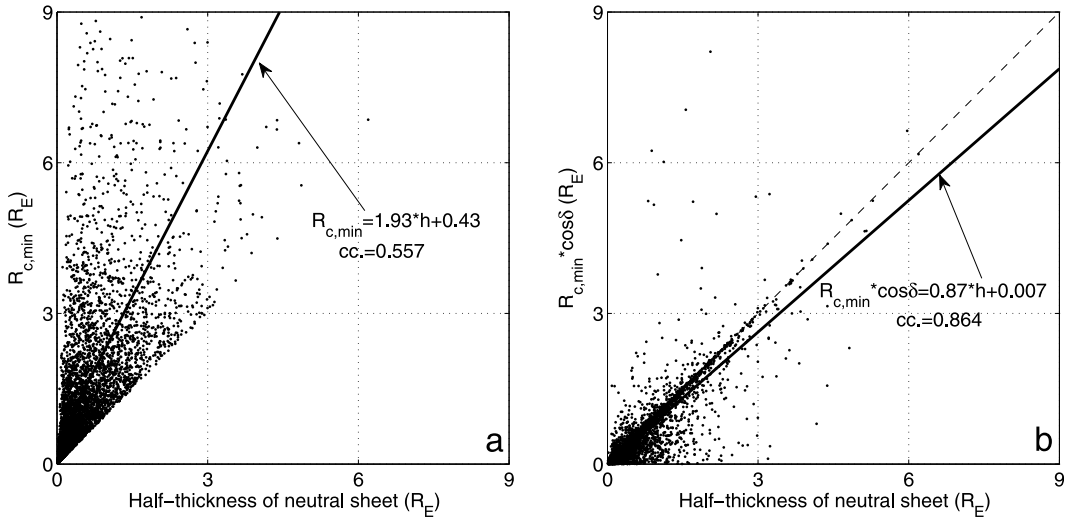

Figure 15. The regression relation between (a) the minimum curvature radius $R_{c,\min}$ and the half thickness of neutral sheet and (b) the minimum curvature radius $R_{c,\min}$ and the modification of slipping angle.

local half thickness of NS, h, which is consistent with the previous case observations [*Shen et al.*, 2008a, 2008b]. Without the modification of slipping angle, the correlation efficient between $R_{c,\min}$ and h is lower (correlation coefficient ~0.56), and there would be no clear relationship between $R_{c,\min}$ and h as argued by *Runov et al.* [2005]. In comparison, as shown in Figure 15b when the slipping angle δ is considered, there is a prominent visually linear trend (indicated by the black dashed line) between $R_{c,\min}$ cos δ and h from the scatter dots, especially when $h > 1\ R_E$. $R_{c,\min}$ cos δ is highly correlated (correlation coefficient ~0.86) with h, and the linear relationship could be estimated as $R_{c,\min}$ cos $\delta \approx 0.87$h with least squares fitting (indicated by the black solid line).

[45] It should be noted that, because of the scattered majority of dots when $h < 1\ R_E$, the fitted line deviates a bit from the visually linear trend. We should recall that the validity of the estimated NS half thickness and the geometric relationship $h = R_{c,\min}$ cos δ is based on the assumption of a 1-D sheet. Therefore, the scattered majority of dots when $h < 1\ R_E$ may imply that some CS cannot be well approximated to be a 1-D sheet, especially for very thin current sheets. Figure 15 demonstrates that h is better correlated with $R_{c,\min}$ cos δ than $R_{c,\min}$, favoring the slipping geometry of MFLs in the CS. Relatively to the thinner CS, h could be well approximated as $R_{c,\min}$ cos δ for the thicker CS ($h > 1\ R_E$).

3.9. The Current Density

[46] With the multipoint observation of Cluster, the current density **j** can be derived via Ampere law, i.e., $\mathbf{j} = \mu_0^{-1}\nabla \times \mathbf{B}$ [e.g., *Chanteur*, 1998; *Dunlop et al.*, 2002a; *Shen et al.*, 2007]. Figures 16a, 16b, 16c, and 16d show the azimuth histogram of the strength of current density j_t and its three components, j_x, j_y, and j_z, respectively, while the ratios j_x/j_t, j_y/j_t, and j_z/j_t are shown in Figures 16e, 16f, and 16g, respectively. It clearly shows that the mean strength of current density at CS center is about $j_t \sim 4$–8 nA/m^2, while near both flank regions the mean strength of j_t is relatively weaker ($j_t \sim 1$–2 nA/m^2). On average, j_x is positive (negative) at the premidnight (postmidnight) region, while j_y is dominant around the midnight region, especially in the range of azimuth angle ~140°–~200°. In comparison with j_x and j_y, j_z is generally weaker and could be neglected. Only in the near-flank region, as indicated by several enhanced bins, j_z is stronger relatively than that around midnight.

[47] Correspondingly, Figure 17 shows the spatially averaged direction (red arrows) of current density, i.e., $\hat{j} = \mathbf{j}/j_t$, that projected onto the *XY* plane (Figure 17a) and *YZ* plane (Figure 17b). It shows clearly that the current density at CS center flows azimuthally from dawn side to dusk side. At the postmidnight region, particularly during the scope $-10\ R_E < Y < 0\ R_E$, the duskward flowing current density has a tailward component, while it has an obvious earthward component at the premidnight region. Around the midnight region $|Y| < 10\ R_E$, current density flows mainly toward the negative Y direction. It interesting to notice that in Figure 7, the direction of current density is basically along the direction of the binormal of MFLs, which would imply the current density might be resulted from the curvature drift motion of charged particles as suggested in earlier studies [e.g., *Zelenyi et al.*, 2004].

[48] It is also interesting to note from Figure 17b that the current density basically seems to be flowing tangential to the CS plane except for the region $Y < -10\ R_E$. Particularly near the dusk flank region, the direction of current density is twisted severely responding to the warped CS.

[49] To check the verticality between the direction of current density, $\hat{j}$, and the normal of CS, $\hat{n}$, it is helpful to define the angle γ_{jn} as the angle between the normal of the CS and the direction of current density, i.e., $\gamma_{jn} = \arccos(\hat{j} \cdot \hat{n})$. Accordingly, Figure 18 shows the histogram of γ_{jn}. It is clear that, for most CS crossing cases, the directions of current density are basically perpendicular to the normal of the CS. If the CS type with $45° < \gamma_{jn} < 135°$ could be seen as the perpendicular type while the remainder is seen as the parallel type, we could find that in total there are 5624 CS crossing events for the perpendicular type (94%) but only 368 CS crossing events for the parallel type (6%). Therefore,

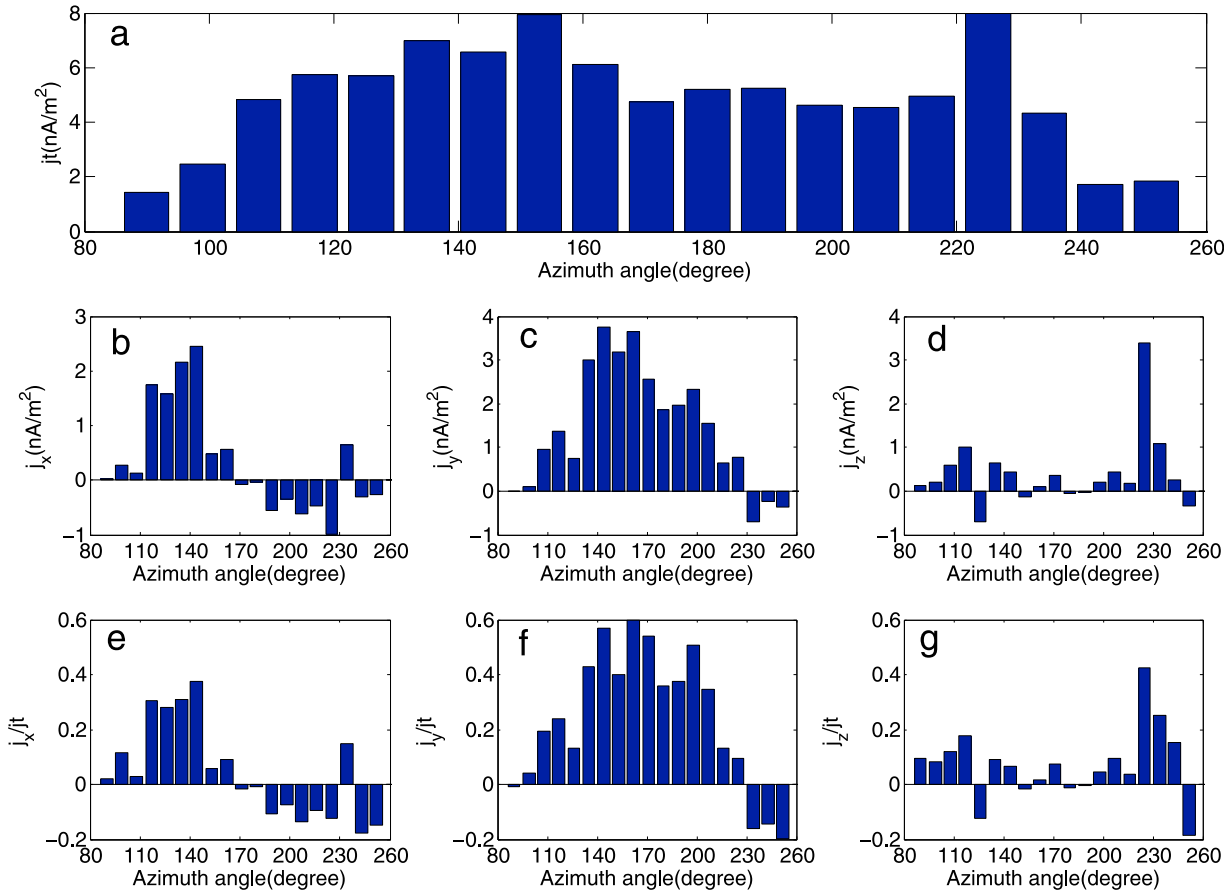

Figure 16. Azimuth histogram of the strength of current density (a) j_t and its three components (b) j_x, (c) j_y, and (d) j_z and for the ratios (e) j_x/j_t, (f) j_y/j_t, and (g) j_z/j_t.

it convinces us that the current density at CS center basically flows tangentially to the surface of tail CS.

[50] Numerous previous studies demonstrate that the current density at CS center basically flows tangentially to the CS, i.e., vertical to CS normal, no matter whether the surface of CS is wavy-like or not [e.g., *Harris*, 1962; *Runov et al.*, 2005, 2006; *Shen et al.*, 2008b; *Rong et al.*, 2010a]. Thus, here it is no wonder that it is possible to observe

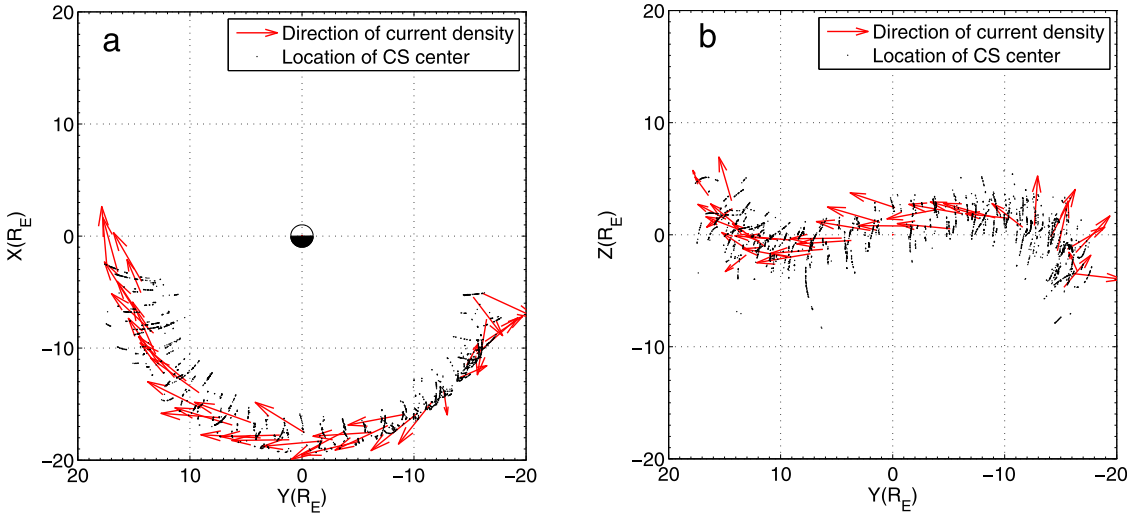

Figure 17. The spatial averaged direction (red arrows) of current density, i.e., $\hat{j} = \mathbf{j}/j_t$ at the CS center as projected onto the (a) *XY* plane and (b) *YZ* plane. The locations of the CS center are shown in black dots in both plots.

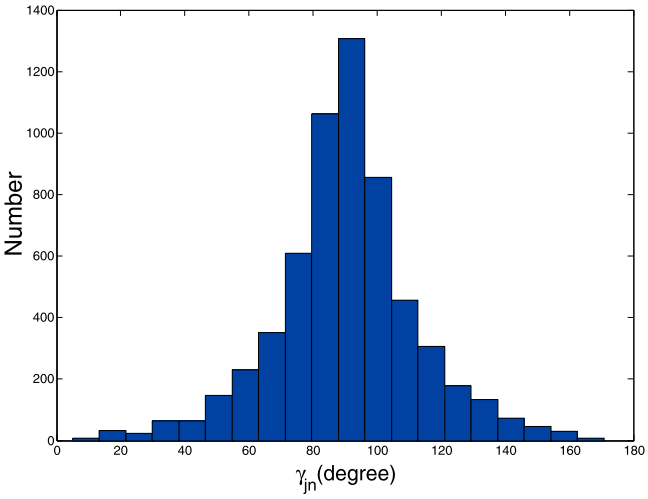

Figure 18. Histogram of the angle between normal of CS and the direction of current density.

statistically the current density at CS center being well tangential to the CS surface.

[51] To explore the reasons why current density flows a bit chaotic and northward pointing near the dawn flank, we checked the current density for the years 2001, 2003, 2004, in detail. We found that for the years 2001 and 2004, the current density flowed relatively well westward from the dawn side to the dusk side. However, for the year 2003, the current density near the dawn flank region ($Y < -10\ R_E$) surprisingly flowed eastward (not shown here). Therefore, we believe that the data points of the year 2003 actually "contaminate" the average orientation of the westward current density and make it bit chaotic and northward pointing near the dawn flank. The plausible reason is that the separation distance of Cluster in 2003 is just about 200 km, so in many CS crossings ($B_x \sim 0$) when near the dawn flank region where the CS is usually thicker, there is no clear stable difference of measured magnetic field between C1, C2, C3, and C4; that is, the current sheet is too thick to be well resolved. Therefore, the "error" current density would probably be derived. To exclude such cases exactly is a troublesome work which has beyond the ability of this study.

4. Summary and Discussion

[52] With the multipoint observations of Cluster on tail CS during 2001, 2003, and 2004, the magnetic parameters, including magnetic field, the 3-D magnetic geometric geometry, the normal of CS, and the current density, at CS center have been statistically studied in detail. The main results are summarized as follows:

[53] 1. At CS center, the B_y component has higher probability of occurring within $|B_y| < 5$ nT, while the B_z component is mostly positive and distributes mainly within 1~10 nT. On average, in the regions with magnetic local times (MLT) ~21:00–~01:00, B_z (3–5 nT) and the minimum magnetic field $B_{\min}$ (5–7 nT) are weaker, but they become stronger near both flanks (B_z, $B_{\min}$, 7–15 nT).

[54] 2. The curvature of MFLs predominantly directs earthward, while the binormal is directed duskward, suggesting that the plane of MFLs is nearly vertical to the equatorial plane.

[55] 3. On the dawn side ($Y < 0$), the curvature direction has a duskward component, while the binormal has a tailward component; on the dusk side ($Y > 0$), the curvature direction has a dawnward component, while the binormal has an earthward component. Such large-scale characteristics demonstrate that the tail magnetic field is flaring.

[56] 4. The negative B_z at CS center has a higher occurrence probability with MLT ~21:00–01:00. The curvature of MFLs associated with negative B_z are predominantly directed tailward.

[57] 5. The CS normal directs mainly along the z axis with some small tilting tailward, suggesting that the surface of the CS could be approximated to a plane with a small tailward tilt.

[58] 6. The tilted CS, with a normal evidently tilting toward the equatorial plane, is observed frequently, which has relatively lower occurrence possibility within the regions with MLT ~21:00–01:00. In the tilted CS, the slippage of magnetic structure is statistically confirmed.

[59] 7. The minimum curvature radius of MFLs, $R_{c,\min}$, that is reached at the CS center, is usually larger than the half thickness of neutral sheet, h. In the range of azimuth angle ~140°–~200°, i.e., MLT ~21:00–01:00, the $R_{c,\min}$(0.6–1 R_E) and h(0.2–0.4 R_E) are relatively smaller, while near both flanks $R_{c,\min}$(3–5 R_E) and h(0.7–1.6 R_E) are relatively larger.

[60] 8. The validity of the geometric relationship $h = R_{c,\min} \cos\delta$ between the minimum curvature radius, $R_{c,\min}$, half thickness of neutral sheet, h, and the slipping angle of MFLs, δ, in the CS is statistically verified.

[61] 9. The current density, with the strength 4~8 nA/m^2, basically flows azimuthally and tangentially to the surface of the CS from the dawn side to the dusk side. At the postmidnight region, in particular $-10\ R_E < Y < 0\ R_E$, the duskward flowing current density has a tailward component, while there is an obvious earthward component at the premidnight region. Around the midnight region $|Y| < 10\ R_E$, current density flows mainly toward the $-Y$ direction.

[62] This work demonstrates clearly that the tail CS has a dawn-dusk asymmetry. In the region between ~21:00~01:00 MLT, the CS is relatively thinner, as indicated by the distribution of B_z, $R_{c,\min}$, and h. The negative B_z has a higher probability of occurrence, which demonstrates that the tail stored energy is more likely to be released there, via magnetic reconnection, current disruption, etc. Accordingly, if the region is mapped to the auroral ionosphere, it is expected that the substorm onset would be optically observed with higher probability at MLT ~21:00–~01:00, which is in agreement with the statistical observations of auroral substorm onset [*Liou et al.*, 2001; *Frey et al.*, 2004]. Figure 19 shows the statistical distribution of auroral substorm onset observed by IMAGE-FUV [*Frey et al.*, 2004], which clearly demonstrates that the auroral substorm onset has higher probability of occurring at MLT ~21:00–~01:00.

[63] The dawn-dusk asymmetry of CS is also consistent with the earlier observations that the tail field lines are found skewed away from the x axis in the dusk side [e.g., *Fairfield and Ness*, 1967; *Mihalov et al.*, 1968]. However, the physical reasons for the CS dawn-dusk asymmetry are still unknown. *Fairfield* [1986] suggested that it might be related to the asymmetric ring current effects; the lower B_z at the

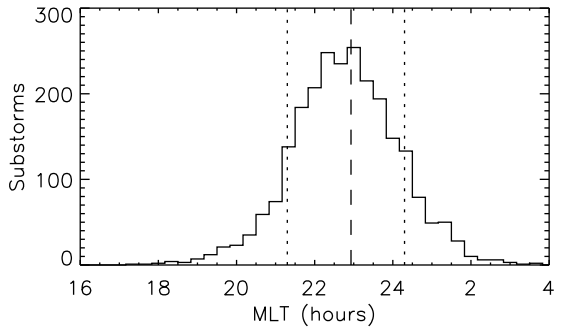

Figure 19. Histograms of the distribution of substorm onsets in geomagnetic longitude, local time (adapted from *Frey et al.* [2004]).

dusk side may be caused by the diamagnetic effect of energetic ions which gradient drift toward dusk when drifting earthward. The CS asymmetry may also imply that the configuration of the downstream magnetopause could show a dawn-dusk asymmetry, but it cannot be completely attributed simply to the Earth's revolution motion as the induced aberration angle is just about 4°.

[64] It is worth noting that the dynamics of the tail CS are assumed to evolve in response to the solar wind conditions or substorm processes. Therefore, though this statistical survey of the magnetic field has been carried out regardless of solar wind and substorms occurrence, it is necessary to study the evolution of magnetic structure responding to the solar wind conditions and the substorm processes in future studies.

[65] **Acknowledgments.** The authors are thankful to the Cluster FGM team and ESA Cluster Active Archive, for providing the publicly available Cluster data. Special thanks to H. U. Frey for providing Figure 19. This work is supported by National Basic Research Program of China (973 Program) grant 2011CB811404 and 2011CB811405, the National Natural Science Foundation of China grant 40974101, 41104114 and 41131066, Specialized Research Fund for State Key Laboratory of Space Weather of the CAS (Chinese Academy of Sciences), China Postdoctoral Science Foundation Funded Project (20100480446), and the Research Fund for the State Key Laboratory of Lithospheric Evolution. The work by M. W. Dunlop is partly supported by CAS visiting professorship for senior international scientists grant 2009S1-54.

[66] Masaki Fujimoto thanks the reviewers for their assistance in evaluating this paper.

References

Baker, D., T. Pulkkinen, V. Angelopoulos, W. Baumjohann, and R. McPherron (1996), Neutral line model of substorms: Past results and present view, *J. Geophys. Res.*, *101*(A6), 12,975–13,010, doi:10.1029/95JA03753.

Balogh, A., et al. (2001), The Cluster magnetic field investigation: Overview of inflight performance and initial results, *Ann. Geophys.*, *19*, 1207–1217, doi:10.5194/angeo-19-1207-2001.

Baumjohann, W., M. Hesse, S. Kokubun, T. Mukai, T. Nagai, and A. Petrukovich (1999), Substorm dipolarization and recovery, *J. Geophys. Res.*, *104*(A11), 24,995–25,000, doi:10.1029/1999JA900282.

Behannon, K. (1970), Geometry of the geomagnetic tail, *J. Geophys. Res.*, *75*(4), 743–753, doi:10.1029/JA075i004p00743.

Büchner, J., and L. M. Zelenyi (1987), Chaotization of the electron motion as the cause of an internal magnetotail instability and substorm onset, *J. Geophys. Res.*, *92*(A12), 13,456–13,466, doi:10.1029/JA092iA12p13456.

Büchner, J., and L. M. Zelenyi (1989), Regular and chaotic charged particle motion in magnetotaillike field reversals: 1. Basic theory of trapped motion, *J. Geophys. Res.*, *94*(A9), 11,821–11,842, doi:10.1029/JA094iA09p11821.

Chanteur, G. (1998), Spatial interpolation for four spacecraft: Theory, in *Analysis Methods for Multi-Spacecraft Data*, edited by G. Paschmann and P. W. Daly, pp. 349–370, Eur. Space Agency, Noordwijk, Netherlands.

Dunlop, M. W., D. J. Southwood, K.-H. Glassmeier, and F. M. Neubauer (1988), Analysis of multipoint magnetometer data, *Adv. Space Res.*, *8*(9–10), 273–277, doi:10.1016/0273-1177(88)90141-X.

Dunlop, M. W., and T. I. Woodward (1998), Multi-spacecraft discontinuity analysis: Orientation and motion, in *Analysis Methods for Multi-Spacecraft Data*, edited by G. Paschmann and P. W. Daly, pp. 271–306, Eur. Space Agency, Noordwijk, Netherlands.

Dunlop, M. W., A. Balogh, K.-H. Glassmeier, and P. Robert (2002a), Four-point Cluster application of magnetic field analysis tools: The curlometer, *J. Geophys. Res.*, *107*(A11), 1384, doi:10.1029/2001JA005088.

Dunlop, M. W., A. Balogh, and K.-H. Glassmeier (2002b), Four-point Cluster application of magnetic field analysis tools: The discontinuity analyzer, *J. Geophys. Res.*, *107*(A11), 1385, doi:10.1029/2001JA005089.

Escoubet, C. P., M. Fehringer, and M. Goldstein (2001), The Cluster mission, *Ann. Geophys.*, *19*, 1197–1200, doi:10.5194/angeo-19-1197-2001.

Fairfield, D. (1979), On the average configuration of the geomagnetic tail, *J. Geophys. Res.*, *84*(A5), 1950–1958, doi:10.1029/JA084iA05p01950.

Fairfield, D. H. (1980), A statistical determination of the shape and position of the geomagnetic neutral sheet, *J. Geophys. Res.*, *85*(A2), 775–780, doi:10.1029/JA085iA02p00775.

Fairfield, D. H. (1986), The magnetic field of the equatorial magnetotail from 10 to 40 R_E, *J. Geophys. Res.*, *91*(A4), 4238–4244, doi:10.1029/JA091iA04p04238.

Fairfield, D. H., and N. F. Ness (1967), Magnetic field measurements with the IMP 2 satellite, *J. Geophys. Res.*, *72*(9), 2379–2402, doi:10.1029/JZ072i009p02379.

Frey, H. U., S. B. Mende, V. Angelopoulos, and E. F. Donovan (2004), Substorm onset observations by IMAGE-FUV, *J. Geophys. Res.*, *109*, A10304, doi:10.1029/2004JA010607.

Fujmoto, M., T. Terasawa, and T. Mukai (1998), The lower-latitude boundary layer in the tail-flanks, in New Perspectives on the Earth's Magnetotail, *Geophys. Monogr. Ser.*, vol. 105, edited by A. Nishida, D. N. Baker, and S. W. H. Cowley, pp. 33–44, AGU, Washington, D. C.

Gloag, J. M., et al. (2010), FGM data products in the CAA, in *The Cluster Active Archive: Studying the Earth's Space Plasma Environment*, edited by H. Laakso, M. Taylor, and C. P. Escoubet, pp. 109–128, Springer, Dordrecht, Netherlands.

Harris, E. G. (1962), On a plasma sheet separating regions of oppositely directed magnetic field, *Nuovo Cim.*, *23*, 115–121, doi:10.1007/BF02733547.

Harvey, C. C. (1998), Spatial gradients and the volumetric tensor, in *Analysis Methods for Multi-Spacecraft Data*, edited by G. Paschmann and P. W. Daly, pp. 307–322, Eur. Space Agency, Noordwijk, Netherlands.

Hughes, W. J., and D. G. Sibeck (1987), On the three-dimensional structure of plasmoids, *Geophys. Res. Lett.*, *14*, 636–639, doi:10.1029/GL014i006p00636.

Kaufmann, R. L., B. M. Ball, W. R. Paterson, and L. A. Frank (2001), Plasma sheet thickness and electric currents, *J. Geophys. Res.*, *106*(A4), 6179–6193, doi:10.1029/2000JA000284.

Liou, K., P. T. Newell, D. G. Sibeck, C.-I. Meng, M. Brittnacher, and G. Parks (2001), Observation of IMF and seasonal effects in the location of auroral substorm onset, *J. Geophys. Res.*, *106*(A4), 5799–5810, doi:10.1029/2000JA003001.

Lucek, E. A., et al. (2005), The magnetosheath, *Space Sci. Rev.*, *118*, 95–152, doi:10.1007/s11214-005-3825-2.

Lui, A. (1996), Current disruption in the Earth's magnetosphere: Observations and models, *J. Geophys. Res.*, *101*(A6), 13,067–13,088, doi:10.1029/96JA00079.

Lui, A. (2003), Cause of magnetospheric substorms, *Plasma Phys. Controlled Fusion*, *45*, 841–852, doi:10.1088/0741-3335/45/6/301.

McComas, C., T. Russell, R. C. Elphic, and S. J. Bame (1986), The near-Earth cross-tail current sheet: Detailed ISEE 1 and 2 case studies, *J. Geophys. Res.*, *91*(A4), 4287–4301, doi:10.1029/JA091iA04p04287.

Mihalov, J., D. Colburn, R. Currie, and C. Sonett (1968), Configuration and reconnection of the geomagnetic tail, *J. Geophys. Res.*, *73*(3), 943–959, doi:10.1029/JA073i003p00943.

Miura, A. (2001), Ballooning instability as a mechanism of the near-Earth onset of substorms, *Space Sci. Rev.*, *95*, 387–398, doi:10.1023/A:1005249915285.

Nakamura, R., W. Baumjohann, A. Runov, and Y. Asano (2006), Thin current sheet in the magnetotail observed by Cluster, *Space Sci. Rev.*, *122*, 29–38, doi:10.1007/s11214-006-6219-1.

Ness, N. F. (1965), The Earth's magnetotail, *J. Geophys. Res.*, *70*(13), 2989–3005, doi:10.1029/JZ070i013p02989.

Ness, N. F. (1969), The geomagnetic tail, *Rev. Geophys.*, *7*(1–2), 97–127.

Øieroset, M., T. D. Phan, M. Fujimoto, R. P. Lin, and R. P. Lepping (2001), In situ detection of collisionless reconnection in the Earth's magnetotail, *Nature*, *412*, 414–417, doi:10.1038/35086520.

Petrukovich, A. A. (2009), Dipole tilt effects in plasma sheet B_y: Statistical model and extreme values, *Ann. Geophys.*, *27*, 1343–1352, doi:10.5194/angeo-27-1343-2009.

Petrukovich, A. A., W. Baumjohann, R. Nakamura, A. Runov, and A. Balogh (2005), Cluster vision of the magnetotail current sheet on a macroscale, *J. Geophys. Res.*, *110*, A06204, doi:10.1029/2004JA010825.

Petrukovich, A. A., T. L. Zhang, W. Baumjohann, R. Nakamura, A. Runov, A. Balogh, and C. Carr (2006), Oscillations of flux tube slippage in the quiet plasma sheet, *Ann. Geophys.*, *24*, 1695–1704, doi:10.5194/angeo-24-1695-2006.

Rong, Z. J., C. Shen, A. A. Petrukovich, W. X. Wan, and Z. X. Liu (2010a), The analytic properties of the flapping current sheets in the Earth magnetotail, *Planet. Space Sci.*, *58*(10), 1215–1229, doi:10.1016/j.pss.2010.04.016.

Rong, Z. J., C. Shen, E. Lucek, A. Balogh, and L. Yao (2010b), Statistical survey on the magnetic field in magnetotail current sheets: Cluster observations, *Chin. Sci. Bull.*, *55*, 2542–2547, doi:10.1007/s11434-010-3096-5.

Runov, A., et al. (2003), Current sheet structure near magnetic X-line observed by Cluster, *Geophys. Res. Lett.*, *30*(11), 1579, doi:10.1029/2002GL016730.

Runov, A., et al. (2005), Electric current and magnetic field geometry in flapping magnetotail current sheets, *Ann. Geophys.*, *23*, 1391–1403, doi:10.5194/angeo-23-1391-2005.

Runov, A., et al. (2006), Local structure of the magnetotail current sheet: 2001 Cluster observations, *Ann. Geophys.*, *24*, 247–262, doi:10.5194/angeo-24-247-2006.

Schwartz, S. J. (1998), Shock and discontinuity normals, Mach numbers, and related parameters, in *Analysis Methods for Multi-Spacecraft Data*, edited by G. Paschmann and P. W. Daly, pp. 249–270, Eur. Space Agency, Noordwijk, Netherlands.

Sergeev, V., D. Mitchell, C. Russell, and D. Williams (1993), Structure of the tail plasma/current sheet at ~11 R_E and its changes in the course of a substorm, *J. Geophys. Res.*, *98*(A10), 17,345–17,365, doi:10.1029/93JA01151.

Sergeev, V., et al. (2003), Current sheet flapping motion and structure observed by Cluster, *Geophys. Res. Lett.*, *30*(6), 1327, doi:10.1029/2002GL016500.

Sergeev, V., A. Runov, W. Baumjohann, R. Nakamura, T. L. Zhang, A. Balogh, P. Louarn, J.-A. Sauvaud, and H. Reme (2004), Orientation and propagation of current sheet oscillations, *Geophys. Res. Lett.*, *31*, L05807, doi:10.1029/2003GL019346.

Shen, C., and M. W. Dunlop (2008), Geometric structure analysis of the magnetic field, in *Multi-Spacecraft Analysis Methods Revisited*, *ISSI Sci. Rep. SR-008*, edited by G. Paschmann and P. W. Daly, chapter 3, pp. 27–32, Int. Space Sci. Inst., Bern, Switzerland.

Shen, C., X. Li, M. Dunlop, Z. X. Liu, A. Balogh, D. N. Baker, M. Hapgood, and X. Wang (2003), Analyses on the geometrical structure of magnetic field in the current sheet based on cluster measurements, *J. Geophys. Res.*, *108*(A5), 1168, doi:10.1029/2002JA009612.

Shen, C., X. Li, M. Dunlop, Q. Q. Shi, Z. X. Liu, E. Lucek, and Z. Q. Chen (2007), Magnetic field rotation analysis and the applications, *J. Geophys. Res.*, *112*, A06211, doi:10.1029/2005JA011584.

Shen, C., et al.. (2008a), Flattened current sheet and its evolution in substorms, *J. Geophys. Res.*, *113*, A07S21, doi:10.1029/2007JA012812.

Shen, C., Z. J. Rong, X. Li, M. Dunlop, Z. X. Liu, H. V. Malova, E. Lucek, and C. Carr (2008b), Magnetic configurations of the tilted current sheets in magnetotail, *Ann. Geophys.*, *26*, 3525–3543, doi:10.5194/angeo-26-3525-2008.

Shi, Q. Q., C. Shen, Z. Y. Pu, M. W. Dunlop, Q.-G. Zong, H. Zhang, C. J. Xiao, Z. X. Liu, and A. Balogh (2005), Dimensional analysis of observed structures using multipoint magnetic field measurements: Application to Cluster, *Geophys. Res. Lett.*, *32*, L12105, doi:10.1029/2005GL022454.

Shi, Q. Q., C. Shen, M. W. Dunlop, Z. Y. Pu, Q.-G. Zong, Z.-X. Liu, E. A. Lucek, and A. Balogh (2006), Motion of observed structures calculated from multi-point magnetic field measurements: Application to Cluster, *Geophys. Res. Lett.*, *33*, L08109, doi:10.1029/2005GL025073.

Slavin, J. A., C. J. Owen, M. M. Kuznetsova, and M. Hesse (1995), ISEE 3 observations of plasmoid with flux rope, *Geophys. Res. Lett.*, *22*, 2061–2064, doi:10.1029/95GL01977.

Speiser, T. W. (1973), Magnetospheric current sheets, *Radio Sci.*, *8*(11), 973–977, doi:10.1029/RS008i011p00973.

Tsyganenko, N. A., and D. H. Fairfield (2004), Global shape of the magnetotail current sheet as derived from Geotail and Polar data, *J. Geophys. Res.*, *109*, A03218, doi:10.1029/2003JA010062.

Tsyganenko, N. A., S. B. P. Karlsson, S. Kokubun, T. Yamamoto, A. J. Lazarus, K. W. Ogilvie, and C. T. Russell (1998), Global configuration of the magnetotail current sheet as derived from Geotail, Wind, IMP 8, and ISEE 1/2 data, *J. Geophys. Res.*, *103*(A4), 6827–6841, doi:10.1029/97JA03621.

Zelenyi, L. M., H. V. Malova, V. Y. Popov, D. Delcourt, and A. S. Sharma (2004), Nonlinear equilibrium structure of thin currents sheets: Influence of electron pressure anisotropy, *Nonlinear Processes Geophys.*, *11*, 579–587, doi:10.5194/npg-11-579-2004.

Zhang, T. L., W. Baumjohann, R. Nakamura, A. Balogh, and K.-H. Glassmeier (2002), A wavy twisted neutral sheet observed by Cluster, *Geophys. Res. Lett.*, *29*(19), 1899, doi:10.1029/2002GL015544.

Zhang, T. L., et al. (2005), Double Star/Cluster observation of neutral sheet oscillations on 5 August 2004, *Ann. Geophys.*, *23*, 2909–2914, doi:10.5194/angeo-23-2909-2005.

M. W. Dunlop, Rutherford Appleton Laboratory, Chilton, Didcot OX11 0QX, UK.

X. Li, Laboratory for Atmosphere and Space Physics, University of Colorado at Boulder, 1234 Innovation Dr., Boulder, CO 80303, USA.

E. Lucek, Blackett Laboratory, Imperial College London, London SW7 2AZ, UK.

A. A. Petrukovich, Space Research Institute, 84/32 Profsoyuznaya st., Moscow 117997, Russia.

Z. J. Rong and W. X. Wan, Beijing National Observatory of Space Environment, Institute of Geology and Geophysics, Chinese Academy of Sciences, Beijing 100029, China. (rongzhaojin@mail.igcas.ac.cn)

C. Shen, State Key Laboratory of Space Weather, Center for Space Science and Applied Research, Chinese Academy of Sciences, Beijing 100190, China.

T. L. Zhang, Department of Geophysics and Planetary Sciences, USTC, 96 Jinzhai Rd., Hefei, Anhui 230026, China.